ENGINEERING RESEARCH

ENGINEERING RESEARCH
ENGINEERING RESEARCH
ENGINEERING RESEARCH
ENGINEERING RESEARCH

FINAL REPORT

FATIGUE BEHAVIOR OF AIR-ENTRAINED CONCRETE

D. Y. Lee
F. W. Klaiber
J. W. Coleman

July 1977

Submitted to the
Highway Division,
Iowa Department of Transportation
HR-183

DEPARTMENT OF CIVIL ENGINEERING
ENGINEERING RESEARCH INSTITUTE
IOWA STATE UNIVERSITY AMES

ISU-ERI-Ames-78017
ERI Project 1259

ERRATA
Final Report HR-183

"Fatigue Behavior of Air-Entrained Concrete"

by
D. Y. Lee, F. W. Klaiber, and J. W. Coleman

July 1977

Page	Line	Now is	Should be
14	6	...with class V aggregate	...with crushed stone & natural sand as aggregates.
	14	2.59	2.66
22	Fig. 5		Delete data point at 5.2% air

TABLE OF CONTENTS

	Page
1. INTRODUCTION	1
1.1 Fatigue of Concrete in Pavement	1
1.2 Air-entrained Concrete in Pavement	6
1.3 Fatigue Behavior of Air-entrained Concrete	8
2. PURPOSE AND SCOPE	10
3. MATERIALS AND PROCEDURES	11
3.1 Test Program	12
3.2 Materials	14
3.3 Mixing Procedures and Quality Control	15
3.4 Equipment	17
4. RESULTS AND DISCUSSION	20
4.1 Physical Properties	20
4.2 Air Content	25
4.3 Microstructure	33
4.4 Results of Fatigue Tests	45
4.5 Treatment of Fatigue Data by Application of Fracture Mechanics	58
4.6 Implications in Concrete Pavement Design	60
5. SUMMARY AND CONCLUSIONS	66
6. RECOMMENDED FUTURE STUDIES	69
7. REFERENCES	70
8. ACKNOWLEDGMENTS	74
9. APPENDIXES	75
9.1 Appendix A. Material Details	76
9.2 Appendix B. Test Data	79
9.3. Appendix C. Pavement Design Calculations	84

LIST OF TABLES

	Page
Table 1. Physical characteristics of concrete studied.	21
Table 2. Air content of concrete by various methods.	29
Table 3. Comparison of pavement design procedures.	64
Table A.1. Gradation of fine aggregate.	76
Table A.2. Gradation of coarse aggregate.	76
Table A.3. Cement properties.	77
Table A.4. Laboratory batch quantities.	78
Table B.1. Test data, Batch C, 2.8% air.	79
Table B.2. Test data, Batch A, 3.5% air.	80
Table B.3. Test data, Batch E, 6.4% air.	81
Table B.4. Test data, Batch D, 10.2% air.	82
Table B.5. Test data, Batch B, 11.3% air.	83

LIST OF FIGURES

		Page
Fig. 1.	Schematic diagram of loading arrangements.	13
Fig. 2.	Photograph of the modulus of rupture test set-up showing support conditions for the third-point flexural loading scheme. Identical support conditions were used in the Instron dynamic cycle for fatigue testing.	18
Fig. 3.	Photograph of the Instron dynamic cycle used for fatigue testing. Note plastic bag around test beam to maintain moist condition.	18
Fig. 4.	Modulus of rupture versus percent air.	22
Fig. 5.	Compressive strength versus percent air.	22
Fig. 6.	Modulus of elasticity versus percent air.	24
Fig. 7.	Unit weight versus percent air.	24
Fig. 8.	High pressure air and linear traverse air vs. plastic state air content.	30
Fig. 9.	High pressure air versus linear traverse air.	32
Fig. 10.	Scanning electron micrographs of concrete specimens taken from end sections of tested beams at about 100 magnification.	34
Fig. 11.	Scanning electron micrographs of concrete specimens taken from end sections of tested beams at about 300 magnification.	35
Fig. 12.	Scanning electron micrographs of concrete specimens taken from end sections of tested beams at about 1000 magnification.	36
Fig. 13.	Cumulative pore volume as percent of bulk volume of concrete versus pore diameter - (non-air-entrained concrete).	41
Fig. 14.	Cumulative pore volume as percent of bulk volume of concrete versus pore diameter - 11.3% air.	41
Fig. 15.	Cumulative pore volume as percent of bulk volume of concrete versus pore diameter of five concretes studied.	42

		Page
Fig. 16.	Cumulative pore volume as percent of total pore volume versus pore diameter - non-air-entrained concrete.	43
Fig. 17.	Cumulative pore volume as percent of total pore volume versus pore diameter - 11.3% air.	43
Fig. 18.	Cumulative pore volume as percent of total pore volume versus pore diameter of five concretes studied.	44
Fig. 19.	Relationship between volume of large mode pores and total air content/porosity.	46
Fig. 20.	Relationship between air content/porosity and median pore diameter.	47a
Fig. 21.	Relationship between volume of mercury retained and total air content/porosity.	47a
Fig. 22.	Relationship between uniformity coefficient and air content/porosity.	47b
Fig. 23.	Photographs of tested beams showing fractured faces.	49
Fig. 24.	S-N curve for 2.8% air concrete.	51
Fig. 25.	S-N curve for 3.5% air concrete.	51
Fig. 26.	S-N curve for 6.4% air concrete.	52
Fig. 27.	S-N curve for 10.2% air concrete.	52
Fig. 28.	S-N curve for 11.3% air concrete.	53
Fig. 29.	Composite S-N curves for five concretes studied.	54
Fig. 30.	Confidence limits for plain concrete with 2.8% and 11.3% air.	55
Fig. 31.	Modified Goodman diagram for plain concrete with 2.8, 6.4, and 11.3% air.	57
Fig. 32.	Pavement fatigue (S-N) design curves.	61

1. INTRODUCTION

1.1. Fatigue of Concrete in Pavement

When a material fails under a number of repeated loads, each smaller than the ultimate static strength, a fatigue failure is said to have taken place. Many studies have been made to characterize the fatigue behavior of various engineering materials. The results of some of these studies have proved invaluable in the evaluation and prediction of the fatigue strength of structural materials. Considerable time and effort has gone into the evaluation of the fatigue behavior of metals. These early studies were motivated by practical considerations: The first fatigue tests were performed on materials that had been observed to fail after repeated loading of a magnitude less than that required for failure under the application of a single load. Mine-hoist chains, railway axles, and steam engine parts were among the first structural components to be recognized as exhibiting fatigue behavior.

Since concrete is usually subjected to static loading rather than cyclic loading, need for knowledge of the fatigue behavior of concrete has lagged behind that of metals. One notable exception to this, however, is in the area of highway and airfield pavement design. Due to the fact that the fatigue behavior of concrete must be understood in the design of pavements and reinforced concrete bridges, highway engineers have provided the motivation for concrete fatigue studies since the 1920's.

Results from fatigue studies are usually presented in the form of an S-N curve (stress versus log of the number of cycles to failure). If there is a break in the curve and the curve becomes asymptotic to a line parallel to the horizontal axis, the stress at which this occurs is called the endurance or fatigue limit. Most metals have an endurance limit; however, tests on concrete up to 10 million cycles of load application have failed to establish an endurance limit.[6] It is therefore important to quote fatigue strength for a specified number of cycles when discussing the fatigue properties of concrete. Fatigue strength is defined as the stress causing failure after a stated number of cycles of loading. Fatigue life is the number of cycles of stress that a specimen can withstand without failure.

The fatigue of concrete is associated with the formation and propagation of microcracks at the aggregate-cement matrix interface and in the cement matrix itself.[6,10,17,43,53] The mechanism of fatigue fracture of concrete is essentially identical to the mechanism of fracture under static and sustained loading.[10] Fatigue fracture involves microcracking similar to, but more extensive than, the microcracking that accompanies static failure. For instance, Bennett[6] found that the total length of surface cracks visible on a concrete specimen subjected to 100,000 cycles of a stress equal to 75% of the static strength was typically 35% greater than the length measured after a single loading to 95% of the static strength.

Most research into the fatigue strength of concrete involves the repeated application of a constant stress until failure (constant stress fatigue). If rest periods are allowed during the test, the

fatigue strength increases. Hilsdorf and Kesler[18] found that rest periods of up to 5 min. after every 10 min. of testing increased the fatigue life from 62 to 68%. One possible explanation of this is concrete's inherent ability to heal cracks in the cement paste.[24] Fatigue life is a function of the range of stress to which the concrete is subjected.[18,33] If a test specimen is subjected to varying stress levels, the fatigue life will also be altered. It is important to understand the effect of varying stress levels because this condition is more representative of the actual condition to which a structural component will be subjected. The fatigue life of a specimen is larger if cyclic loading at a high stress level is followed by cyclic loading at low stress level. If the lower stress level is applied first, a decrease in fatigue life is observed. A relatively low number of cycles of high loads can increase the fatigue life of concrete under a lower load beyond the life of a specimen which has not been previously loaded.[18] This increase in fatigue life can be attributed to the fact that concrete exhibits two opposing effects when loaded: consolidation and consequent strengthening and microcracking and consequent weakening. The controlling effect will depend on the relative magnitude and method of application of the loads. Many other factors affect the fatigue strength of concrete; among these are aggregate type and quality, moisture condition, rate of loading, age of concrete at testing, type of loading, concrete strength, curing conditions, specimen size, and air entrainment.[22,36,38]

Highway concrete slabs are subjected to many repetitions of traffic loads during their service lives; thus, the importance of fatigue in concrete pavement is self-evident. Since the flexural stresses in

concrete pavement slabs are critical, fatigue due to flexural stress is used for concrete pavement design. Fatigue tests in compression, although useful for many design applications, do not provide information useful to the designer of pavements. Loading schemes which subject concrete specimens to flexural loading more realistically duplicate conditions encountered in the field.

The first fatigue tests using flexure specimens were carried out by Féret in 1906.[36] These tests, although similar to later investigations, are only of historical value due to more recent and complete research. Two extensive investigations on flexural fatigue of concrete were carried out by Purdue University (1922-24) and the Illinois Department of Highways (1921-23). The Illinois tests reported by Clemmer[11,37] and the Purdue tests served as a basis for the development of the Portland Cement Association (PCA) design curve for fatigue strength of concrete pavement in 1933.[45]

Clemmer devised a unique testing machine in which 6 in. x 6 in. x 36 in. concrete beams were cantilevered out from a central hub. Load was applied by rotating a pair of rubber-tired wheels about the central hub. Blocks were placed between the cantilevered beams to form a smooth circular track. Load applied by the wheels could be varied by placing dead weight in two weight boxes located on the axle between the two wheels. Test beams were subjected to 40 load applications per minute. Clemmer found that the endurance limit for concrete was between 51 and 54% of the modulus of rupture, as determined from a static test, for up to 2 million cycles of load application. As was previously

stated, more recent investigations have not shown the existence of a fatigue limit in concrete, at least up to 10 million cycles of load application.

Hatt[16] at Purdue University carried out flexural tests significantly different from Clemmer's but came to similar conclusions. Specimens, 4 in. x 4 in. x 30 in., were tested as cantilever beams. Each specimen was subjected to stress reversal at a rate of 10 cycles/min. by a test machine which applied load by weights alternately lowered on the opposite ends of a cross member fastened to the end of the beam. Hatt felt that 40 applications of load per minute used by Clemmer was too fast to compare with actual road conditions. Testing was also shut down overnight to allow for rest periods to better duplicate field conditions.

Of special significance is the fact that the fatigue response of concrete in the laboratory was also reflected in actual pavement performance and in results of field road tests in terms of decrease of serviceability index and development of cracks with increasing number of load applications.[9,20,39,40,48,52]

The most widely used fatigue curves for plain concrete pavement design are those of the Portland Cement Association.[13,45] The derivation and history of these curves will be elaborated later in the text. The current PCA curve, adopted in 1966, can be expressed as follows:

$$SR = 0.972 - 0.0828 \log N$$

where

SR = stress ratio

= ratio of flexural stress to modulus of rupture

and

N = number of allowable load repetitions.

Virtually all modern rigid pavement design methods recognize the importance of the fatigue life of concrete and, in design, consider not only the anticipated weights but also the number of heavy axle loads which will be applied during the pavement design life. These methods, for example, the AASHTO Interim Design Procedure[1] used by most highway departments in this country, and the Road Note 29 design procedure[2] used in the United Kingdom are also based on road test data. The major input of both methods is the total number of equivalent 18-kip single axle loads applied during the design life. The PCA design procedure evaluates the accumulated fatigue effects of all heavy axle load applications during the pavement life to prevent slab cracking.

In summarizing the preceding discussions on concrete fatigue and rigid pavement design, the following can be concluded:

- Concrete, used in pavement slabs, is subjected to fatigue failure.
- Concrete pavement performance and distress is a function of load repetitions; therefore, load repetitions have a direct influence on the thickness requirements of a concrete pavement.
- Virtually all modern rigid pavement design methods take into consideration the fatigue strength (fatigue life and load repetitions) of concrete.

1.2. Air-entrained Concrete in Pavement

The use of admixtures which cause the entrainment of air in concrete is considered by many to be one of the most important developments

in concrete technology in the last few decades. The principal application has been to pavement concrete. Entrained air benefits concrete mainly in two ways: (1) improved resistance of the concrete to freezing and thawing and (2) improvement of the workability and decrease in segregation of freshly mixed concrete. Air bubbles present in the cement paste of unhardened concrete can come from several sources[28]: (1) air originally present in intergranular spaces in the cement and aggregate, (2) air originally present within the particles of cement and aggregate but expelled from the particles before hardening of the concrete by inward movement of water under hydraulic and capillary potential, (3) air originally dissolved in the mixing water, and (4) air which is in-folded and mechanically enveloped within the concrete during mixing and placing. These are the only sources of air bubbles in concrete, whether or not an air-entraining agent is used.[28] An air-entraining agent makes use of the fourth method of supplying air bubbles to a plastic concrete mix. Air-entraining agents reduce the surface tension at air-water interfaces within the cement paste which reduces the rate of dissolution of air in the bubbles and the tendency of bubbles to join together, forming larger bubbles. This produces a uniform distribution of very small air bubbles within the cement paste matrix. It is this distribution of bubbles that accounts for the increased freeze-thaw durability as well as the decreased compressive and tensile strengths of air-entrained concrete. These and other effects of the air void system in concrete have been well documented.[28,29,30,31]

Today air-entrained concrete is recommended for all structures under conditions of severe exposure and for all pavements regardless of climatic conditions.[19,25,45,51] Depending on the maximum size of aggregate, the usual recommended entrained air content varies from 5% for a 2-in. aggregate to 8% for a 1/2-in. aggregate.[46] For pavement concrete the specified air content in Iowa is 6 ± 1½%.[44]

In recent years, because of the greatly increased use of de-icing chemicals, it has been found necesary to incorporate higher levels of air in concrete to assure freedom from deterioration due to frost action (in certain instances, air content of 8 or 9% has been recommended for use in structures such as highway bridge decks). Furthermore, there is reason to suspect that, because of the concern on the part of the contractor that he achieve the desired workability and meet minimum air content requirements, the actual air content in field placed concrete could, in some cases, be higher than recommended.

1.3. Fatigue Behavior of Air-entrained Concrete

The effects of air content on most concrete properties such as compressive strength, workability, durability, and creep are quite well understood. For example, it is known that, for normal levels of air content, if there is no change in water-cement ratio the strength will be reduced by 3 to 5% for each percent air added. However, knowledge of the effect of air content on the flexural fatigue strength of plain concrete is nearly nonexistent. In view of recent nationwide interest in economical pavement design, data must be collected on the effects of all

additives and variables on the fatigue strength of concrete.

A literature search of the past 70 years produced only two reported studies on the fatigue strength of air-entrained concrete. One of the studies was carried out in 1943 by Purdue University for the Kentucky Department of Highways.[14] It involved flexural fatigue testing of beam specimens in which one of the variables was air entrainment. The fatigue life of the air-entrained concrete was slightly greater than non-air-entrained groups. This finding is only of limited interest, however, since the different groups that were compared contained different cements, and the variable of air content was not singled out for comparison. Also, the load histories of the test beams varied, making a comparison of fatigue lives difficult. In the second study, Antrim and McLaughlin[4] performed axial compression fatigue tests on two types of concrete, one air-entrained and the other containing only natural air. This study resulted in two major conclusions:

1. The fatigue behavior of non-air-entrained plain concrete and air-entrained plain concrete in compression are not significantly different. However, there is an indication that air-entrained concrete exhibits longer fatigue life at low stress ratios (less than about 77% of static compressive strength) and shorter fatigue life at higher stress levels.

2. There is considerably less variation present among fatigue test data for air-entrained plain concrete than there is for non-air-entrained concrete.

This study is of interest since an air-entrained concrete was included, although at only one air-content level. However, the failure of highway pavements is essentially a tensile failure, and this study involved loading of specimens in compression; thus, an assumption of the behavior of concrete pavement based on the results of this study would be a dangerous extrapolation of the findings.

2. PURPOSE AND SCOPE

While all of the modern pavement design procedures recognize the importance of fatigue life of concrete and air entrainment is being used for all concrete pavements, design curves currently being used in the design of portland cement concrete pavements do not reflect the effect of air entrainment. The basic fatigue data, on which concrete pavement designs have been based for the past 40 to 50 years, were derived in early 1920's, 20 years before the introduction and 40 years before the widespread use of air-entrained concrete. No data are available on the fatigue behavior of air-entrained concrete in flexure.

In light of the extensive use of air entrainment and the growing interest in economy and efficiency of design, it becomes self-evident that, in order to properly design concrete pavements, a study of the effects of air entrainment on the fatigue behavior of concrete in flexure is urgently needed. The purpose of this study is to evaluate the effects of air entrainment on the fatigue strength of plain concrete and establish preliminary fatigue curves for air-entrained concrete to be used in concrete pavement design.

The scope of this work includes flexural fatigue testings of concretes at various levels of air entrainment, prepared with one aggregate and grading, one cement type, and at one water-cement ratio.

3. MATERIALS AND PROCEDURES

3.1. Test Program

The objective of this investigation was to determine the effect of varied air content on the flexural fatigue strength of plain concrete. To optimize the research effort, the test program was designed with air content as the only independent variable. All other variables such as age of concrete when tested, water-cement ratio, aggregate type, curing conditions, temperature, and cement type were held constant. A total of five laboratory mixes with air content as the only variable were studied.

The age variable was eliminated by testing all batches at an age of 28 to 56 days. This meant that a concrete batch was mixed and poured approximately once each month. After the initial 28-day period when the first batch was curing, fatigue testing proceeded at a continuous rate. The first batch was tested at the same time the second batch was curing. At the end of the 28-day period, testing of the first batch was completed, the third batch was poured, and testing of the second batch began. This cycle was continued until testing of all five batches was complete.

The original test program failed to allow for machine down time, in that problems with the fatigue machine were encountered during testing of the first batch. Because of this, Batch A was actually tested at an age of 48 to 97 days. Batches B through E were tested according to the schedule outlined above. As will be demonstrated later, the age variable (in Batch A) had no effect on the fatigue behavior up to 97 days.

Beams for fatigue testing were 6 in. x 6 in. x 36 in. A modulus of rupture test was performed on the first 18 in. of the beam (Fig. 1a) and a fatigue test on the remaining unstressed portion (Fig. 1b). This procedure provided a companion modulus of rupture test for each individual fatigue test. After the modulus of rupture test and prior to the fatigue testing each beam was sealed in a plastic bag to maintain a saturated moist condition. Previous studies[38] have found that if the beams are allowed to air dry during fatigue testing the scatter of the data will increase. This is believed to be due to differential strains generated by moisture gradients within the beam.

The stress level for fatigue testing of each specimen was arrived at by taking a percentage of the modulus of rupture. This stress level was then converted to an equivalent load to be applied to the beam. Fatigue testing consisted of repeated applications of this constant equivalent load until failure occurred. Fatigue tests were made at four stress levels corresponding to 90, 80, 70, and 60% of the modulus of rupture. Six specimens were tested at each stress level, corresponding to an anticipated 95% confidence limit.[23,27]

The main fatigue test program was supplemented by five additional investigations; these investigations were centered around the following subjects:

1. Modulus of rupture tests,
2. Compressive strength tests,
3. Modulus of elasticity determination,

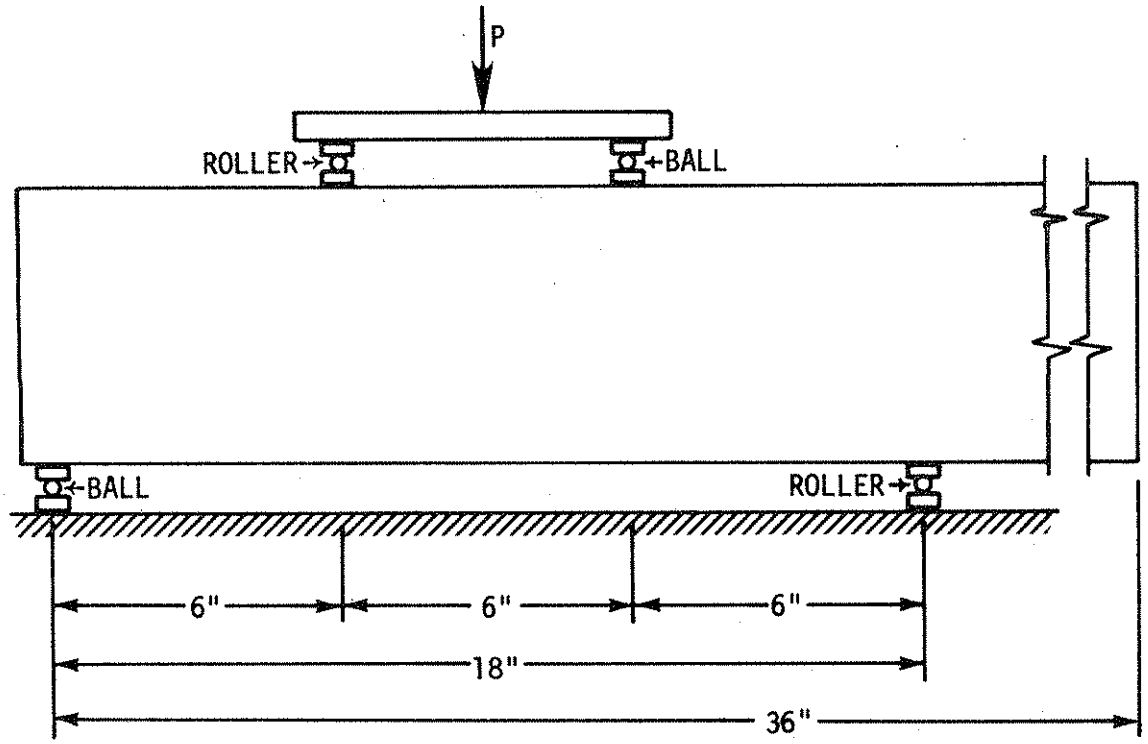

A. MODULUS OF RUPTURE TEST

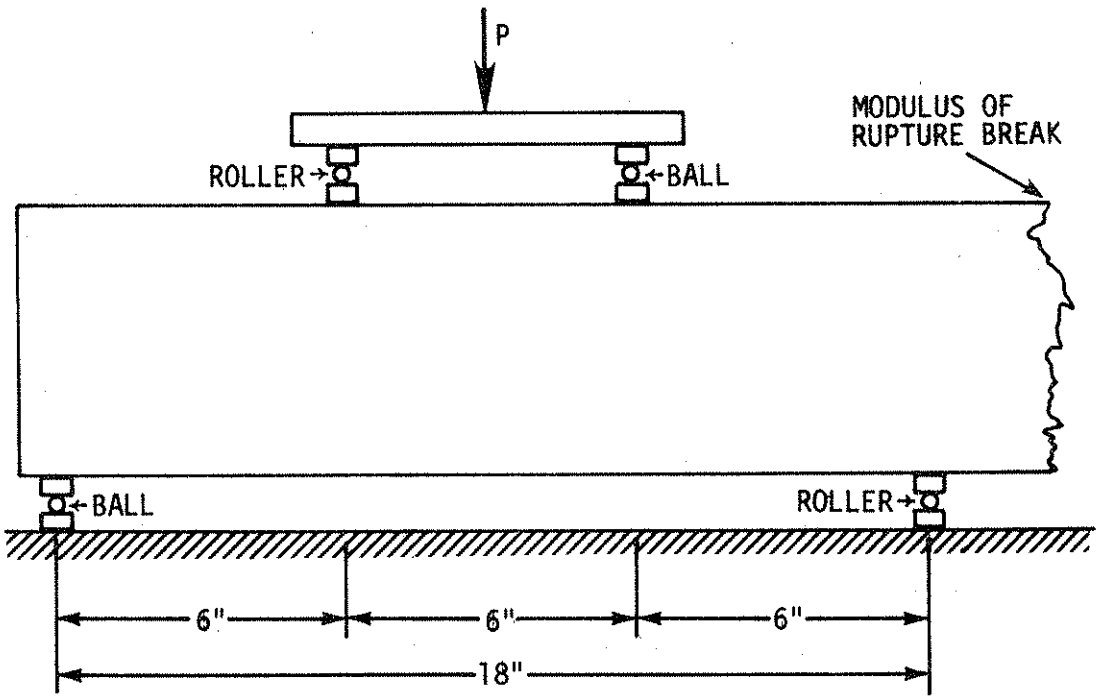

B. FATIGUE TEST

Fig. 1 Schematic diagram of loading arrangements.

4. Comparison of air determination methods, and
5. Concrete microstructure by scanning electron microscopy and mercury penetration porosimry.

3.2. Materials

Concrete used for laboratory test specimens consisted of an Iowa Department of Transportation C-3 mix with Class V aggregate.[44] The water-cement ratio used was .41 for all batches, slightly less than 0.43 called for in Iowa specifications. Coarse aggregate consisted of crushed limestone from the Alden quarry near Alden, Iowa. Fine aggregate (concrete sand) was obtained from Hallett Construction Company in Ames, Iowa. Both coarse and fine aggregates came from Iowa D.O.T. approved stockpiles. The coarse aggregate had a saturated-surface-dry specific gravity of 2.55 and absorption of 2.46%. The fine aggregate had a saturated-surface-dry specific gravity of 2.59 and water absorption of 1.33%. Further information regarding aggregate gradation and specifications can be found in Tables A-1 and A-2 of Appendix A and reference 44. As may be observed in the tables, the coarse and fine aggregates utilized meet the Iowa D.O.T. specifications. Type 1 Portland cement used in the concrete batches was obtained from Marquette Cement Corporation in Des Moines, Iowa. In order to guarantee uniformity, care was taken to assure that all the cement was taken from one batch at the cement plant. Chemical and physical properties of the cement are given in Table A-3 of Appendix A.

Ad-Aire, a vinsol resin produced by the Carter Waters Company of Kansas City, Missouri (recommended by the engineers of the Iowa D.O.T.),

was used as the air-entraining agent for all laboratory mixes. Trial batches were run to determine the amount of air-entraining agent to use for a specified air content. It was found that this amount varied with respect to age. Due to this variation it was necessary to run trial batches prior to each concrete pour to determine the amount of air-entraining agent and other batch quantities necessary for the desired air content.

3.3. Mixing Procedures and Quality Control

The laboratory portion of the investigation consisted of five different series of test specimens in which the only variable was the amount of air. In one batch of concrete no air-entraining agent was added, so that the only air would be the natural air, which is a function of mixer type, amount of concrete mixed compared to mixer capacity, etc. This non-air-entrained batch was used as the control for comparison purposes. Each batch (A - E) consisted of approximately 30 fatigue beams 6 in. x 6 in. x 36 in., approximately six modulus of rupture beams 6 in. x 6 in. x 30 in., and fifteen 6-in. diameter x 12 in. cylinders. Approximately 1 1/2 cubic yards of concrete were required in each batch for preparation of the required test and control specimens.

Because uniformity of mix was of the utmost importance, all mixing was carried out in the laboratory. Since no mixer of this capacity was available, a ready-mix transit mixer was rented and brought into the laboratory. Before the batch quantities were charged into the mixer, the mixing drum was carefully inspected to determine if there was any

left-over concrete or mixing water left in the drum which would alter the desired mix. This procedure allowed strict control of the concrete batch quantities throughout the mixing procedure. Batch quantities (see Table A-4 of Appendix A) were weighed, corrected for moisture content, and charged into the empty mixing drum. After completion of a predetermined mixing time, the slump and plastic air content of each batch was measured and recorded. The fresh concrete was then transferred to the beam molds by wheelbarrow. All mixing procedures utilized were in accordance with ASTM C 192. Flexural specimens were vibrated according to ASTM C 192 using a small laboratory type pencil vibrator with a 1-in. head which operated at 10,500 vibrations per minute. As the concrete was being placed in the forms control cylinders were cast in 6 in. by 12 in. waxed cardboard cylinder molds that were filled with concrete representative of that in the beams.

Immediately after initial set the beams and cylinders were covered with wet burlap and heavy polyethylene sheet to assure proper and uniform curing conditions.

After an initial curing period of 24 to 48 hours, the forms were stripped and the beams removed. They were then transferred to large metal tanks where they were stored submerged in water until testing.

Air content determination tests were performed on the fresh concrete using standard air meters of the pressure type throughout the investigation (ASTM 231).[12] In addition to the Iowa State University air meters, two air meters were borrowed from the Iowa Department of Transportation for comparison. Both sets of meters were calibrated prior to, and used only for, this investigation. Air meter readings from both sets of meters

were in close agreement throughout the test program. For consistency all plastic air tests were performed by one operator throughout the investigation. Fresh air contents were later compared with hardened air contents obtained by high pressure[26] and linear traverse methods.[7]

3.4. Equipment

Modulus of elasticity and compression tests were performed on a 400^k universal testing machine. ASTM standards C 39 and C 469[12] were adhered to during all tests. A concrete cylinder compressometer was used for determination of the modulus of elasticity. The 400^k test machine in conjunction with a one-third point load fixture (see Fig. 2) was used for modulus of rupture tests. The overhanging portion of the test specimen caused an insignificant amount of stress of opposite sense at the critical test section and thus its effect is negligible. After the modulus of rupture test, the longer portion of the test specimen, which was approximately 24 in. long, was placed in an Instron Model 1211 dynamic cycler for fatigue testing. The portion of the beam used in the fatigue test was the overhang portion of the beam and thus was stress free in the modulus of rupture test. The Instron was modified so that flexural one-third point loading was applied (Fig. 3). As may be seen in Fig. 1b, the loading on the test specimen is at the same spacing as in the modulus of rupture test (Fig. 1a). The dynamic cycler has a $\pm$ 20,000 lb force capability with the ability to test from 0 to 15,000 lb in tension. The frequency of load application can be varied from 5 to 35 cycles/sec. All tests during this investigation

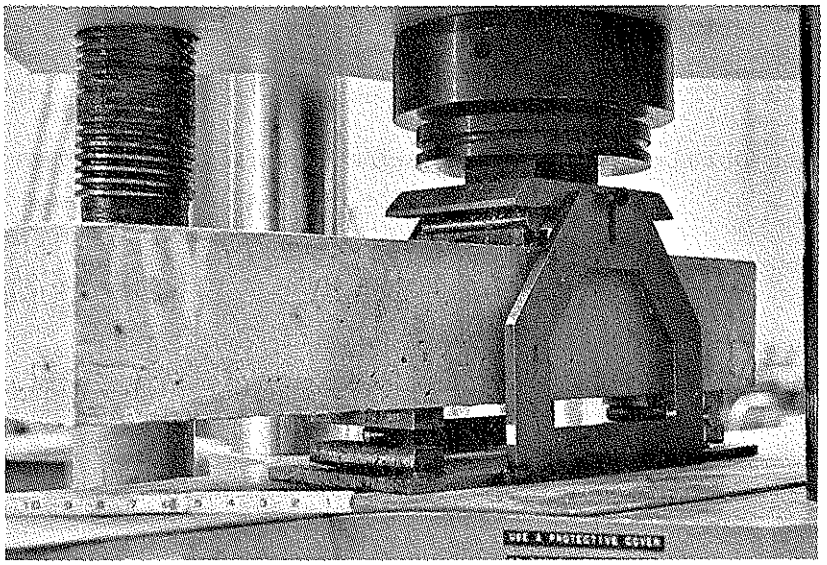

Fig. 2 Photograph of the modulus of rupture test set-up showing support conditions for the third-point flexural loading scheme.

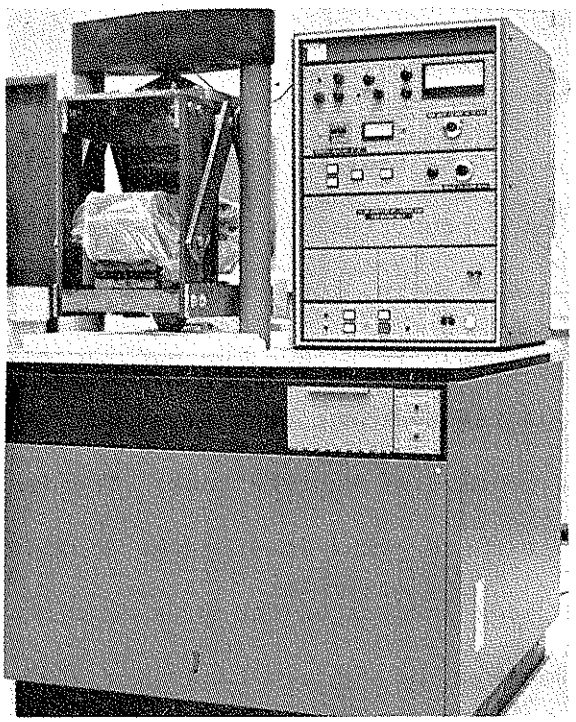

Fig. 3 Photograph of the Instron dynamic cycle used for fatigue testing. Note plastic bag around test beam to maintain moist condition.

were run at 5 to 7.5 cycles/sec. Kesler[21] has shown that speed of testing between 70 and 440 cycles/min. has a negligible effect on the fatigue strength of plain concrete. The bottom fibers of the specimens were subjected to a nominal minimum load to tension load cycle for fatigue testing with tension corresponding to the maximum flexural load applied.

Air contents of hardened concrete by high pressure air meter and by linear traverse methods were performed at Iowa D.O.T. laboratories with Iowa D.O.T. equipment.

Microstructures of hardened concrete were studied using a JEOL JSM-U3 scanning electron microscope and a Micromeritics Model 905-1 mercury porosimeter.

4. RESULTS AND DISCUSSION

4.1. Physical Properties

In the following sections the experimentally determined physical characteristics for the five batches of concrete tested in this study are presented. A summary of the concrete properties are presented in Table 1. The 28-day compressive strength presented is the average of three compression tests, modulus of elasticity value is the average of two tests, and the modulus of rupture value is the average of all beams tested in each batch. Note that the data presented in Table 1 is in order of increasing air contents. Batch designations represent order of pour, i.e., A was first, B second, and so forth.

4.1.1. Modulus of Rupture

In addition to modulus of rupture stresses obtained in the fatigue beams, two modulus of rupture tests were performed per each additional beam in order to establish the degree of variability within and between the various beams of a given batch. It was found that occasionally a significant difference would occur (up to 12%); however, the difference between companion breaks was usually less than 3%. The method of supplying a companion static test for each fatigue test is felt to be the most accurate when dealing with a nonhomogeneous material such as concrete.

The results of the modulus of rupture tests are plotted in Fig. 4. The curve shown represents a log-log regression analysis with a correlation coefficient (r) of -0.99. The equation of the line is:

Table 1. Physical characteristics of concretes studied.

Batch	% Air	Slump, in.	Unit Weight, pcf	28-day Compressive Strength, psi	Modulus of Elasticity-psi x 10^6	Modulus of Rupture, psi
C	2.8	1.00	149.9	5365	5.03	862.8
A	3.5	1.25	146.7	5000	4.24	817.9
E	6.4	4.50	140.1	3650	3.23	582.3
D	10.2	5.00	132.4	2608	2.66	482.3
B	11.3	3.75	133.1	2728	2.33	508.5

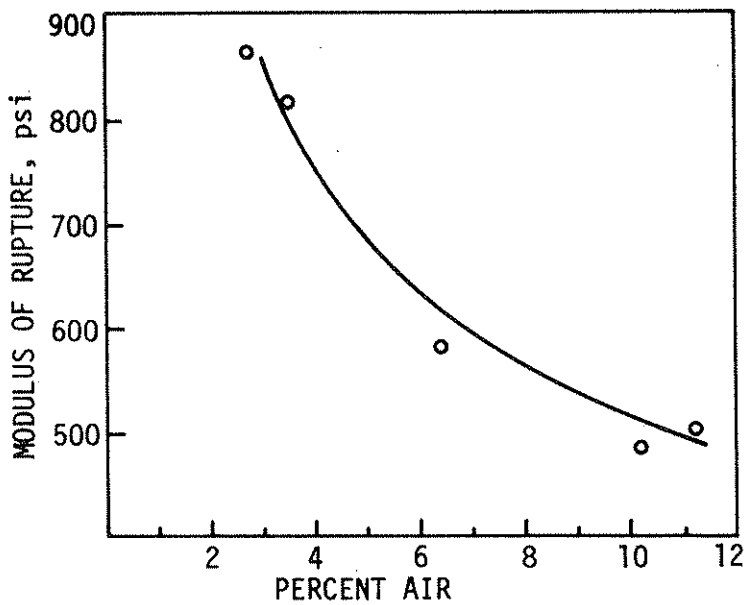

Fig. 4 Modulus of rupture vs percent air.

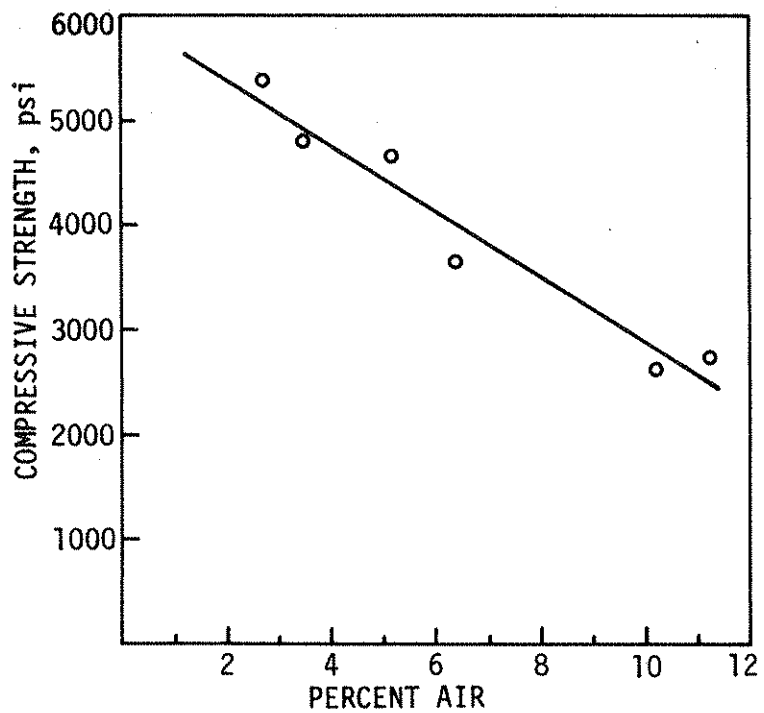

Fig. 5 Compressive strength vs percent air.

$$f_r = 1337.09 \text{ Pa} - 0.42$$

where f_r is the modulus of rupture and Pa is the percent air. (Henceforth, "percent of air" refers to plastic air content unless otherwise stated.) Modulus of rupture values observed in the laboratory are higher than can be expected in the field, due primarily to the superior curing conditions available in a laboratory environment. The results of these tests show that as the air content of concrete increases the modulus of rupture decreases at a second-order rate. This finding agrees with the general relationship between tensile strength of concrete and the square root of the compressive strength.

4.1.2. Compressive Strength

Results of the 28-day compressive tests are shown in Fig. 5. The line represents a linear regression analysis, the equation of which is:

$$f'_c = 313.95 \text{ Pa} + 6000$$

where f'_c is the 28-day compressive strength, Pa is the percent air, and the correlation coefficient (r) is -0.98. From these tests it can be concluded that the compressive strength of concrete decreases linearly as air content increases, about 300 psi or 6 to 12% decrease in strength for each percent of air added.

4.1.3. Modulus of Elasticity

As the amount of entrained air in a concrete specimen goes up the elastic behavior of the concrete is altered. Fig. 6 shows the effect of air on the modulus of elasticity of plain concrete.

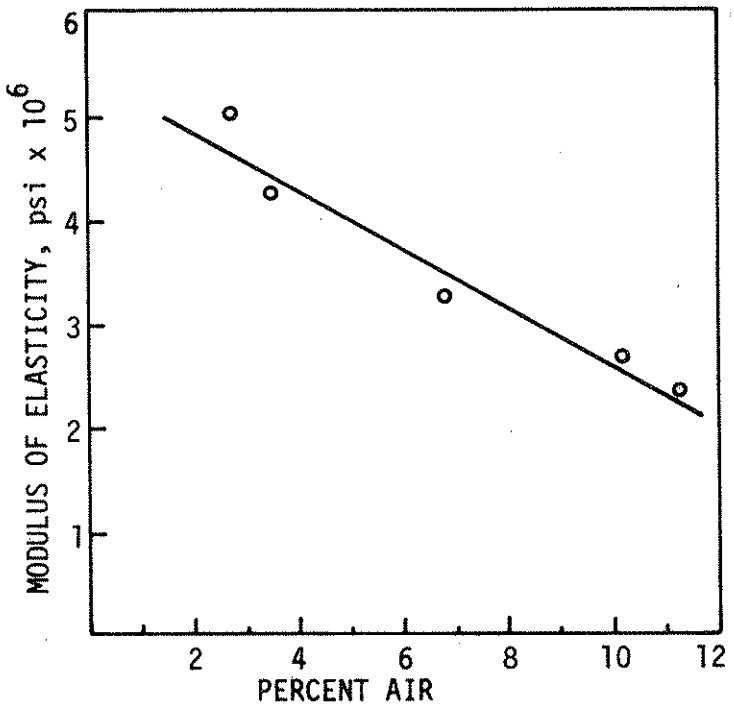

Fig. 6 Modulus of elasticity vs percent air.

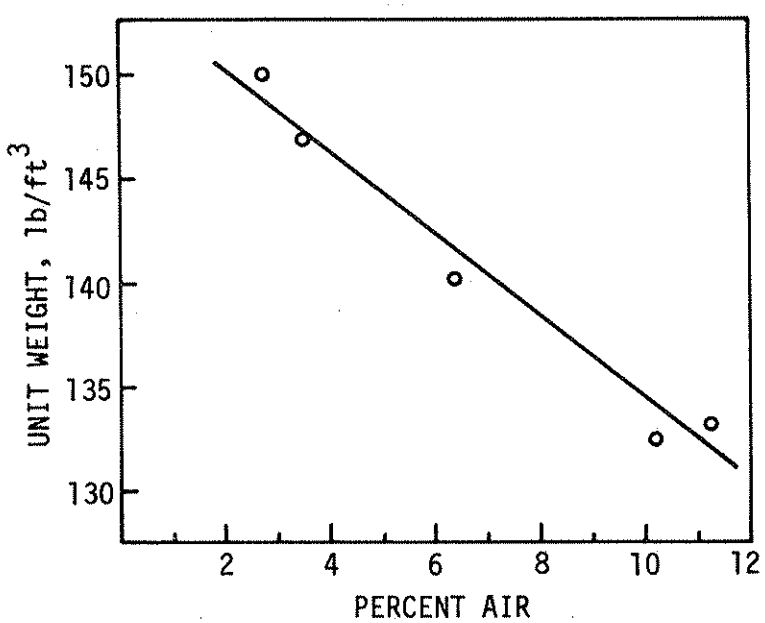

Fig. 7 Unit weight vs percent air.

The equation of this line is:

$$E_c = -0.28\ Pa + 5.42$$

where Pa is the percent air in the concrete, the correlation coefficient (r) is -0.96, and E_c is the modulus of elasticity in 10^6 psi. Modulus of elasticity tests were made using a standard concrete cylinder compressometer with a dial gage attachment. The elastic modulus was determined by taking the difference between strain readings at 354 and 1768 psi stress. These values correspond to 10,000 and 50,000 lb loads, respectively.

4.1.4. Unit Weight

The results of the unit weight determinations are shown in Fig. 7. A loss in unit weight of approximately 2 lb/cu ft accompanied the addition of 1% air.

4.2. Air Content

The benefits of air entrainment in concrete with respect to freeze-thaw, salt-scaling resistance, and workability have been discussed earlier. Depending on the maximum size of aggregate (and therefore on the amount of air bubbles in mortar), the usually recommended total air content ranges from about 5% for a 2-in. aggregate to about 8% for a 1/2-in. aggregate.

Although total air content is specified and measured in current practice, the more important air void property influencing concrete durability is a parameter called the spacing factor, i.e., the average distance from any point in the paste to the periphery of the nearest

air bubble. As the spacing factor decreases, the freeze-thaw durability increases. It has been found that for proper durability a maximum spacing factor of about 0.01 in. is required. Warren[3] has shown that the void-spacing factor is decreased by about half when air content is increased slightly above that obtained without using an air-entraining agent. For air contents greater than about 3% the void-spacing factor decreased only slightly with an increase in air content of from 3 to 8%. This finding indicates that there is little advantage in increasing air content beyond about 4%, especially in view of the reduction in strength with increase in air content. On the other hand, it is possible, although unlikely, to obtain the recommended total air content but not the desired protection against freeze-thaw action if the bubbles are too large and not well distributed throughout the mortar component of the concrete.

From the above discussion the following can be concluded:

1. There exists an optimum range of air contents which gives the desirable qualities of durability and workability without undue loss of strength.

2. There is a need for a better or alternate method of specifying, measuring, and controlling air content in concrete other than total air content.

Air content of concrete in the plastic state can be measured by the pressure method (ASTM C 231), the volumetric method (ASTM C 173), or the gravimetric method (ASTM C 138). The air content of hardened concrete can be measured by the high pressure air method[26] or various microscopic methods; among these are the point count method, the areal traverse method, and the linear traverse method.[31,41]

An Iowa Department of Transportation high pressure air meter was used for determining the air content of 4-in. diameter hardened concrete cores drilled from end sections of tested fatigue beams. Cores were first oven dried for 72 hrs at 300°F, and then cooled for a period of 3 hrs. After weighing, the cores were soaked in water for 48 hrs. The cores were then weighed in water, removed and patted dry with a cloth, and weighed again in air to determine the water absorption. With specimen preparation complete, the cores were placed in the high pressure air meter. Pressure of approximately 5000 psi was then applied to the specimen chamber by means of a cylinder piston. A dial reading was recorded from which the air content of the core could be computed. Detailed information concerning the high pressure air tests can be obtained by consulting Test Method No. Iowa 407-A, April 1971, Iowa Department of Transportation, Materials Department.

Linear traverse air content determinations were performed according to ASTM C 457, with a few modifications as noted below. Specimens were also cut from the end section of tested fatigue beams using a diamond saw. The same beams were used to obtain linear traverse specimens and high pressure air specimens. Each linear traverse sample was polished with wet silicon carbide paper of grades 120, 240, 320, 400, and 600. Polishing time was approximately 15 min. for each grade except the 120 grade which was applied for 30 min. A total traverse of 100 in. was obtained from a minimum area of 24 sq. in. Minimum distance between traverses was taken as 0.2 in. All measurements were made at a magnification of 50 times. Both total and less than 1 mm diameter air contents were determined, the latter being considered

by many as the upper limit of "entrained air." To determine voids less than 1 mm in diameter, the counter reading corresponding to 1 mm was determined. A traverse was first completed for total air, and then all voids larger than 1 mm or parts thereof were counted along the same traverse. The amount of less than 1 mm air was then determined by taking the difference between these two readings. Spacing factors were also calculated based on equations given in ASTM C 457.

The results of air content determinations are given in Table 2.

High pressure air meter results are compared with plastic air contents in Fig. 8. The line shown represents a linear regression analysis of the data with a correlation coefficient of 0.99. The equation of the line is

$$HA = 1.28\ Pa + 0.25$$

where HA is high pressure air content and Pa is plastic air content.

Linear traverse results are also compared with plastic air contents in Fig. 8. The linear traverse curve represents a linear regression with a correlation coefficient of 0.99. The equation of the line is

$$LT = 1.15\ Pa - 0.28$$

where LT is linear traverse percent air and Pa is the plastic air content. Although there is no agreement on the differences between entrapped and entrained air, if for discussion purpose air voids larger than 1 mm are called "entrapped air" and air voids less than 1 mm are referred to as "entrained air," the following statements can be made.

Table 2. Air content of concrete by various methods.

Batch	Average Plastic % Air	Average High-Pressure % Air	Average Linear Traverse % Air < 1 mm	Average Linear Traverse % Air Total	Spacing Factor, in.
C	2.8	3.4	1.08	2.61	.0362
A	3.5	4.5	---	3.55	.0410
E	6.4	9.4	5.99	7.89	.0096
D	10.2	13.0	10.59	11.51	.0045
B	11.3	14.5	10.51	12.32	.0040

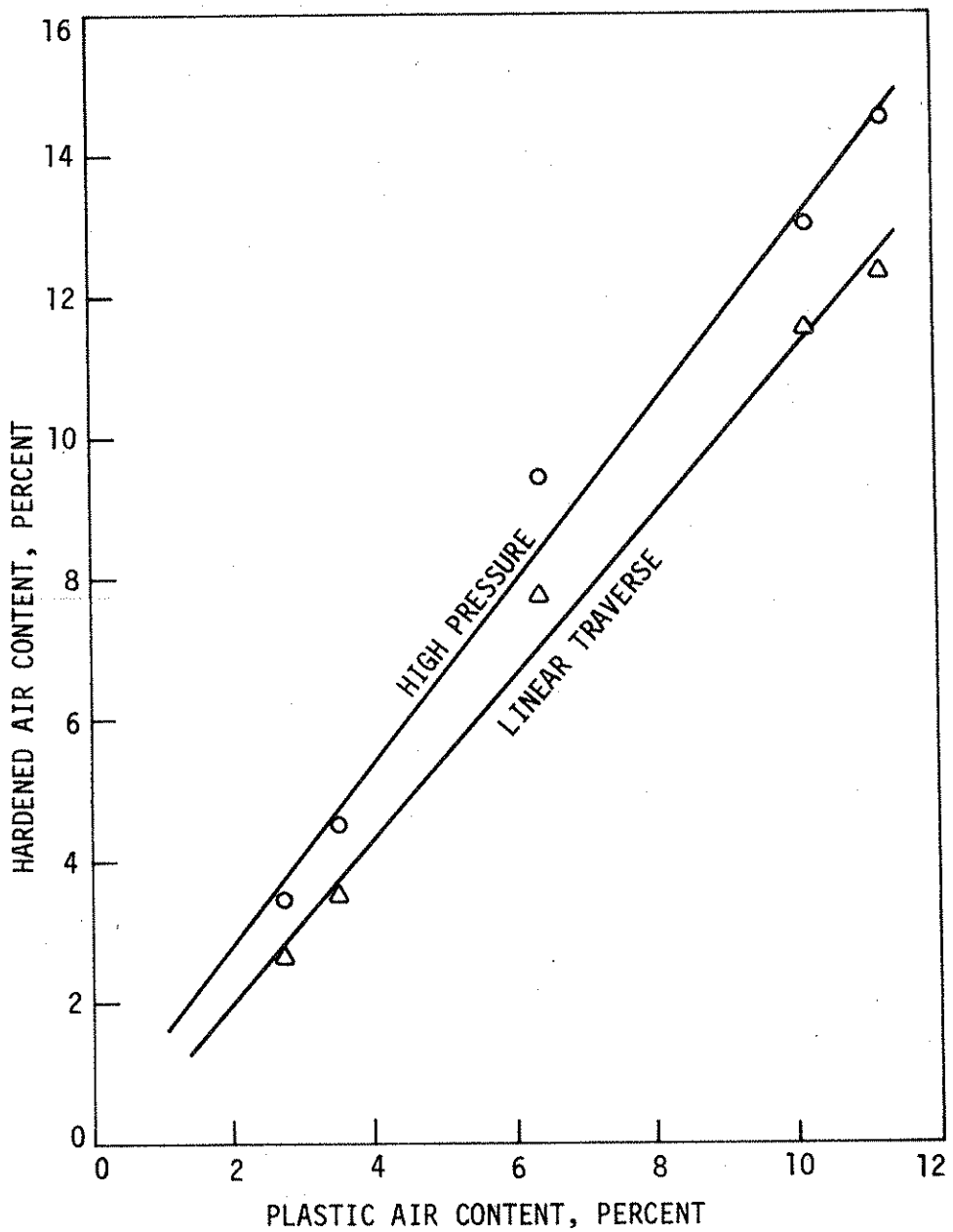

Fig. 8 High pressure air and linear traverse air vs plastic state air content.

The percent "entrapped air" (larger than 1 mm) ranged from 0.9 to 1.9 with an average of 1.5 and was independent of total "entrained air" (less than 1 mm) content. Spacing factor ranged from 0.0362 in. for 2.8% air (non-air-entrained) concrete to 0.0040 in. for 11.3% air concrete. Except for one case, both high pressure air and linear traverse methods yielded results higher than the original plastic air content, especially at higher air content levels. This is in general agreement with findings of other investigators.

Results of the high pressure air tests are compared with linear traverse results in Fig. 9. Again the curve represents a linear regression analysis with a correlation coefficient of 0.998. The equation of the curve is

$$HP = 1.11\ LT + 0.56$$

where HP is high pressure percent air and LT is linear traverse percent air. Air content values determined by the high pressure method were consistently higher.

The coefficient of determination, r^2, for all three curves is very close to 1.00, indicating a good linear data fit.

Since pavement specifications are written on the basis of plastic air content, curves of this type are useful in establishing the original plastic air content any time after placement of a concrete pavement.

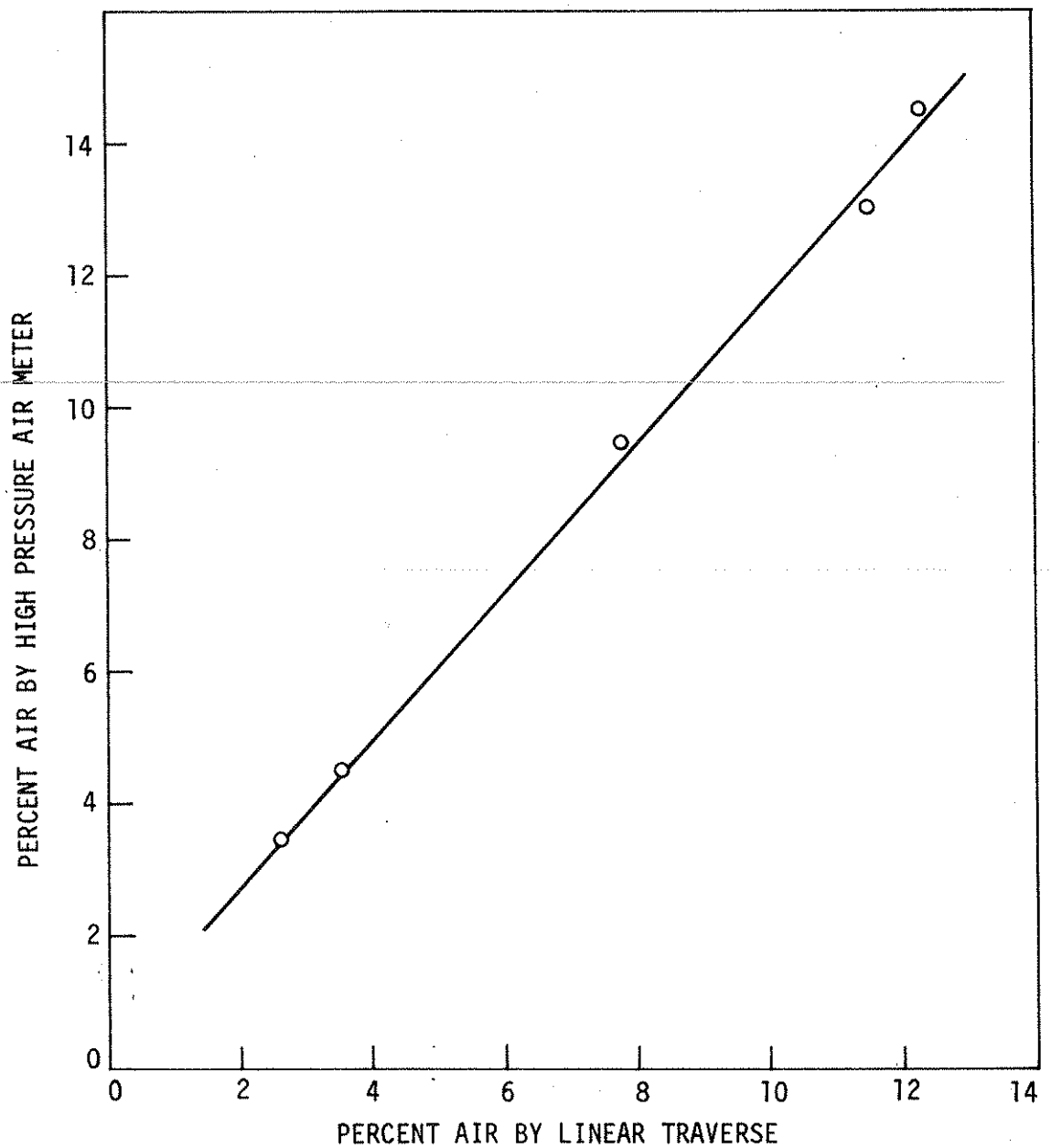

Fig. 9 High pressure air vs linear traverse air.

4.3. Microstructure

4.3.1. Scanning Electron Microscopy

A JEOL/JSM-U3 scanning electron microscope was used to visually examine the microstructure of hardened concrete specimens from all batches. The purposes were: (1) to establish the differences, if any, between entrapped and entrained air, (2) to determine the effect of air entrainment on the pore structure and pore size distribution, and (3) to examine the microcracks in the cement paste matrix caused by stress.

The relative size of entrained versus entrapped air is a subject that few authorities agree on. Neville[35] indicates that entrained air is of the magnitude of 0.5 mm (0.02 in.), with a range between 0.5 and 1.30 mm (0.002 and 0.05 in.), while entrapped air forms much larger bubbles. Other authorities give varying parameters for the differentiation between entrained and entrapped air. Among those who believe there is a size difference between entrapped and entrained air, the dividing size seems to be 1.00 mm.

Scanning Electron Microscope photographs are shown in Fig. 10, 11, and 12. All specimens observed under the scanning electron microscope were taken from end sections of beams subjected to fatigue loading at 70% of the static modulus of rupture.

Figure 10 shows the size, shape, and size distribution of air bubbles of typical non-air-entrained (2.8% air), normal air-entrained (6.4% air), and high air-entrained (11.3% air) concrete at about 100 magnification. Figures 11 and 12 show micrographs of the same

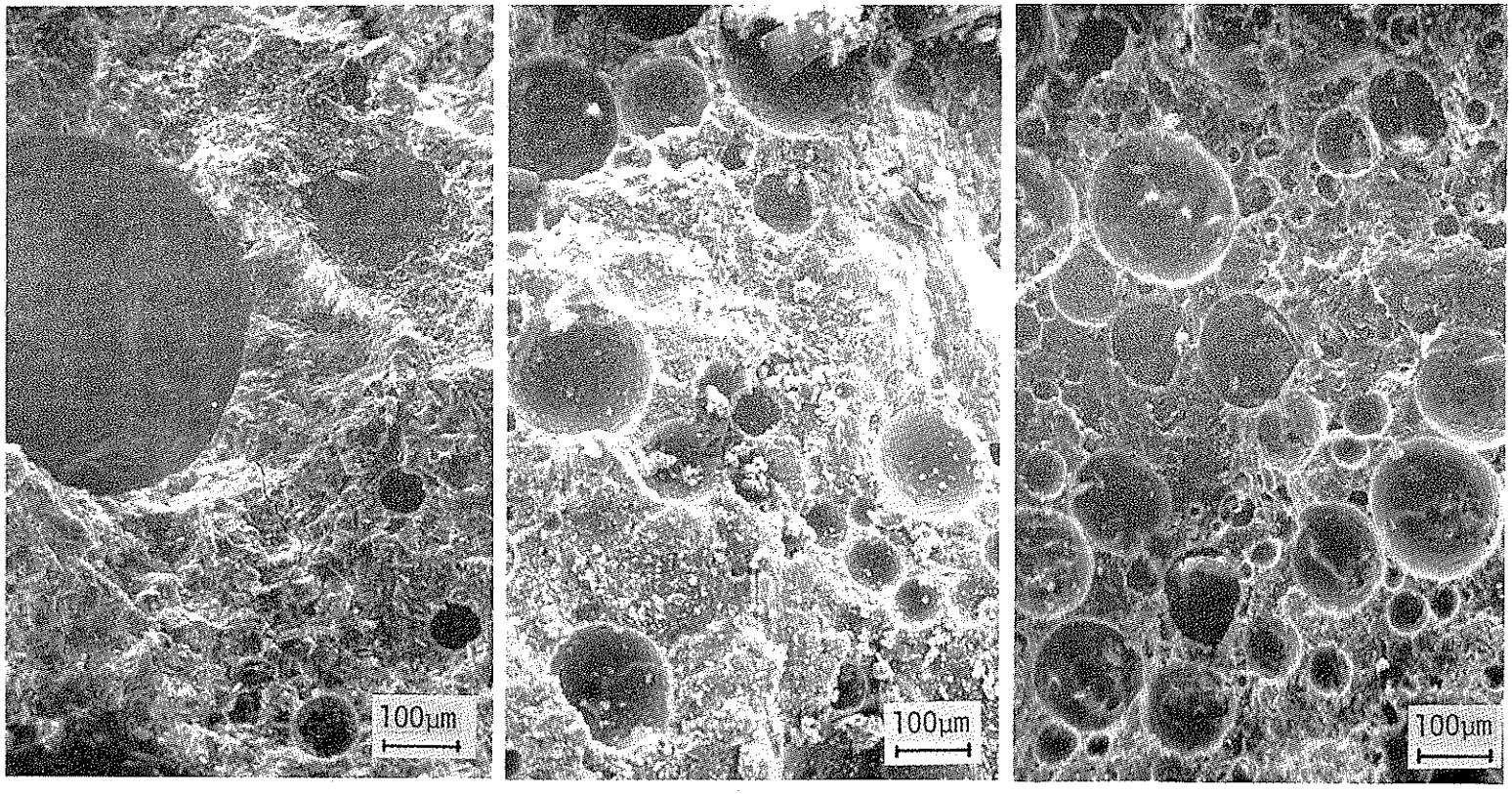

(A) 2.8% AIR (NON-AIR-ENTRAINED)
SPACING FACTOR = 0.0362 IN.
(0.92 mm)

(B) 6.4 AIR
SPACING FACTOR = 0.0096 IN.
(0.24 mm)

(C) 11.3% AIR
SPACING FACTOR = 0.0040 IN.
(0.10 mm)

Fig. 10. Scanning electron micrographs of concrete speciments taken from end section of tested beams (× 100).

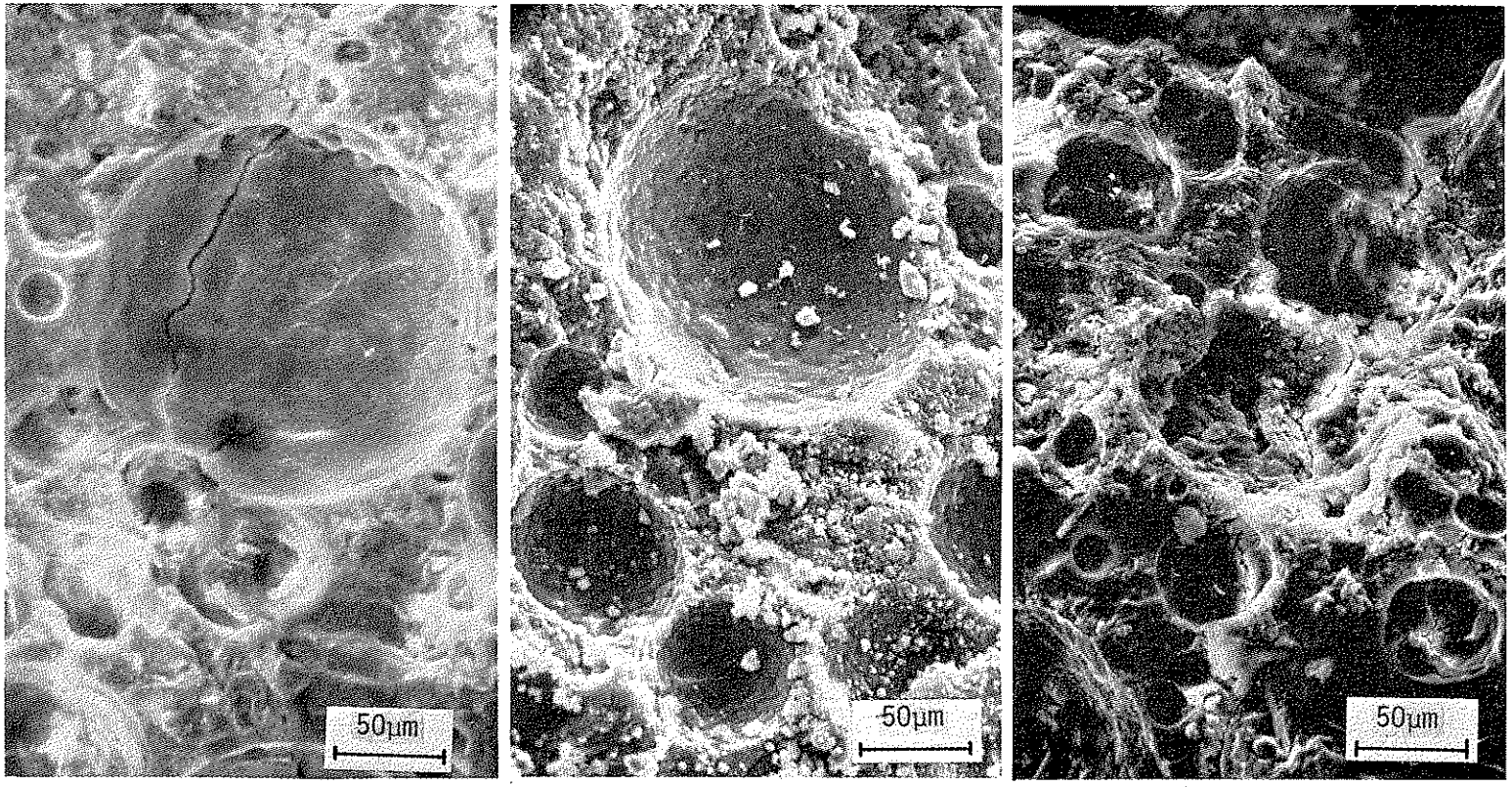

(A) 2.8% (NON-AIR-ENTRAINED) (B) 6.4% AIR (C) 11.3% AIR

Fig. 11. Scanning electron micrographs of concrete specimens taken from end section of tested beams (× 300).

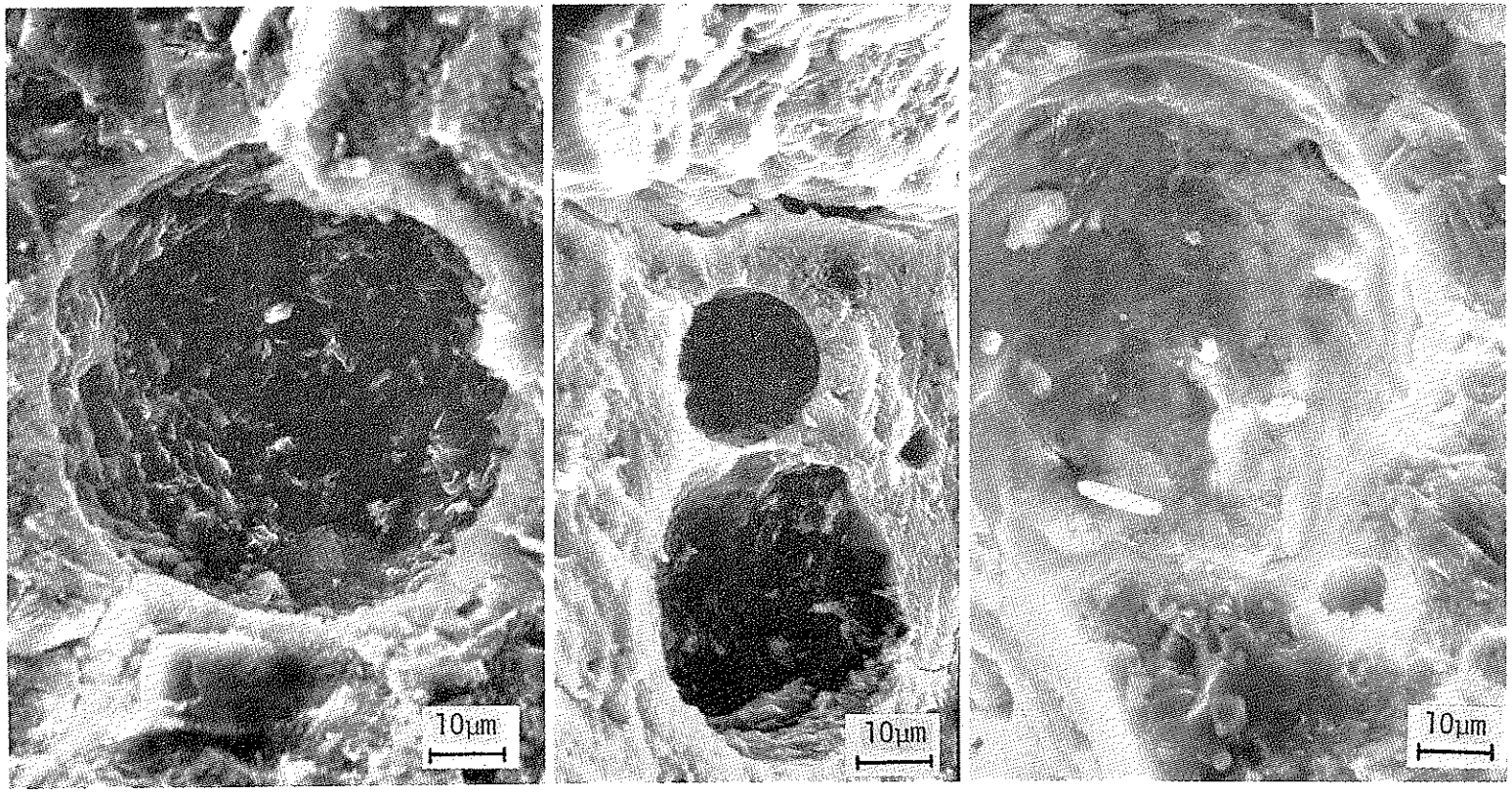

(A) 2.8% AIR (B) 3.5% AIR (C) 11.3% AIR

Fig. 12 Scanning electron micrographs of concrete specimens taken from end sections of tested beams (× 1000).

three concretes at about 300 and 1000 magnifications. Details of Fig. 10a is shown in Fig. 12a and those of Fig. 10b and c are shown in Figs. 11b and c.

The introduction of air-entraining agent increased the number of bubbles, the bubble density, and the uniformity of air bubbles; this is most evident from Fig. 10. The spacing factors are indicated for visual comparison. Air bubbles in air-entrained concrete consist of a uniform distribution of very small air voids, mostly between 0.02 and 0.10 mm (20 and 100 μm); few are as large as 0.2 mm and some are as small as 0.005 mm (5 μm), and are usually spherical in shape. However, air bubbles as large as 1.5 mm, although not shown in the micrographs presented, have been observed. The interior of most air bubbles is usually smooth in appearance. The air bubbles of the non-air-entrained concrete can usually be characterized by a lack of intermediate size bubbles, presence of large bubbles (as large as 2 mm), and by bubbles of more irregular shapes and rough interior texture (Fig. 12a). However, smooth, spherical air bubbles of sizes in the range found in air-entrained concrete can also be found (Fig. 11a). From these micrographs it is difficult to conclude that there is a dividing line between entrained and entrapped air based on size and shape. The differentiation between entrained and entrapped air should, therefore, be based on intent and effect rather than a strict size determination. Entrained air is a uniform network of small air voids intentionally placed in a concrete mix. Entrapped air can be any size air void naturally present in the material and/or caused by mixing action or improper compaction. Entrapped air, due to its

uneven distribution, and its often large size and spacing factor, does not have a beneficial effect on freeze-thaw durability.

As shown in Figs. 10a, 11a, 11c, and 12, microcracks can be observed in specimens subjected to stress. Fatigue behavior of metals is based on crack propagation and growth on a microscopic scale. Microcracks in concrete have been observed under dynamic as well as static loads.[10] It would seem that some parallel could be drawn between the fatigue behavior of metals and concrete. In order for this to be done the initiation and propagation of microcracks in concrete must be well documented and understood. This subject should be pursued in future studies to better understand the fatigue behavior of concrete.

4.3.2. Pore Size Analysis by Mercury Porosimetry

Most of the important properties of hardened concrete, especially strength and durability, are influenced by the quantity, size, and size distribution of various types of pores in the concrete. In an attempt to characterize and quantify the pores of concrete specimens with various air content, mercury porosimetry was used.

The principle of the mercury penetration technique is quite simple. The size and quantity of pores in solid materials are measured by determining the quantities of a nonwetting liquid - mercury - that is forced into the pores under investigation at various pressures. The equation describing the penetration of mercury into pores under pressure is given by Washburn[49]:

$$pr = -2\sigma \cos \theta$$

where p is the pressure applied, r the pore radius, σ the surface

tension of mercury, and θ the contact angle of the mercury with respect to the solids. Specimens used in this study were concrete cores, 1 in. long by 1 in. diameter, drilled from slices cut from the end section of test beams. Prior to placing the specimen in the sample cell of the porosimeter, the concrete core is soaked in acetone for several hours to remove lubricant used in drilling and then oven-dried. The sample cell, containing the specimen, is then placed in the pressure chamber of the mercury porosimeter. A vacuum is used to evacuate the chamber so that the pressure gages will indicate the net pressure, p, used in the Washburn equation. Once the pressure chamber is evacuated, mercury is let into the chamber, filling the sample cell and immersing the specimen. Knowing the volume of the mercury which flows into the sample cell and the volume of the sample cell, it is possible to calculate the bulk volume of the sample. As pressure is applied, mercury intrudes the specimen. Both the volume of mercury which intrudes the specimen and the corresponding pressure are measured. Using these data in the Washburn equation, it is possible to compute the radius of pore which is being intruded at a given pressure.

After completion of the pressurization/mercury penetration measurements, a de-pressurization/mercury retention can be run. Mercury expelled from pores as a function of decreasing pressure can be measured. This gives information about the shape and structure of the pores.

The porosimeter used in this study was a Micromeritics Model 905-1 Mercury Penetration Porosimeter. It has a pressure range from about 2.7 to 50,000 psi for large sample cell. Using a mercury surface tension of 474 dyn/cm at 25°C and a contact angle with concrete of 130°, it is

possible to measure pore diameters between 32.7 and 0.00354 μm.

At least three cores were tested from each batch. The results are presented in two ways: (a) cumulative pore volume distribution curves (Figs. 13, 14, and 15) and (b) cumulative pore volume as percent of total pore volume versus pore diameter curves (Figs. 16, 17, and 18).

In discussing mercury penetration results and comparing them with air content results of hardened concrete measured by conventional methods, the following should be noted:

- As indicated in pore size distribution curves the maximum pore size detected by mercury penetration technique is about 10 μm, which is the lower limit of air bubbles which can be measured by conventional air content determinations.

- The calculated pore diameter is the equivalent diameter of the pore entrance ("pore entry diameter") of interconnected or open pores; the total volume of pore may not include all isolated discrete air bubbles.

- The pore volume of the concrete specimens included pores in the paste (capillary and gel pores), pores in the aggregate, "under-aggregate" fissures,[47] and, in some cases, stress-induced microcracks.

Recognizing the above characteristics of mercury penetration data, the following can be observed:

1. In spite of the heterogeneous nature of the concrete material dealt with and the limitations of the small sample sizes, the results, as seen in Figs. 13 and 14, are surprisingly reproducible.

2. At low air entrainment (2.8 and 3.5% air), the added air had essentially no effect on the pore structure of cement paste. The total porosity of the concrete can be attributed to the porosity of the aggregate and capillary/gel pores (see Fig. 15).

3. At a total air content larger than 3.5%, as the air content increases, there is an increase in total porosity and pore volume (Figs. 15 and 18). This increase was mainly reflected in the volume of "large" (1 to 10 μm) pores with little effect on smaller pores (between 1 and 0.008 μm), corresponding

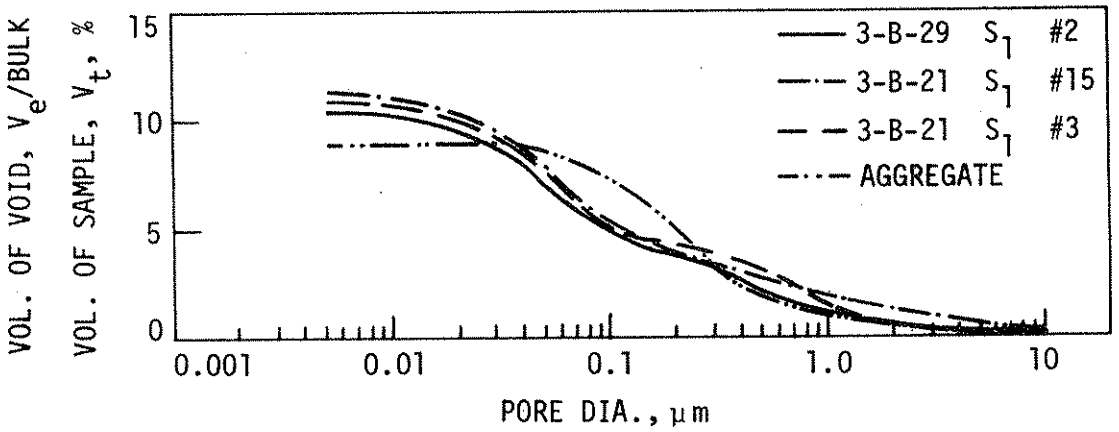

Fig. 13 Cumulative pore volume as percent of bulk volume of concrete vs pore diameter - (Non-air-entrained concrete).

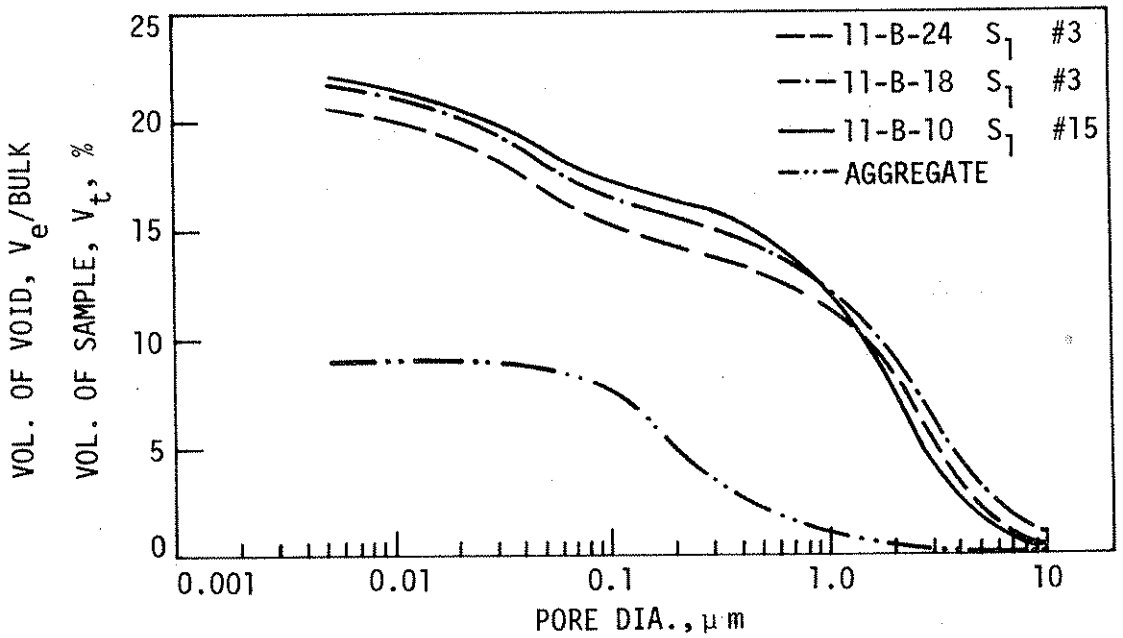

Fig. 14 Cumulative pore volume as percent of bulk volume of concrete vs pore diameter - 11.3% air.

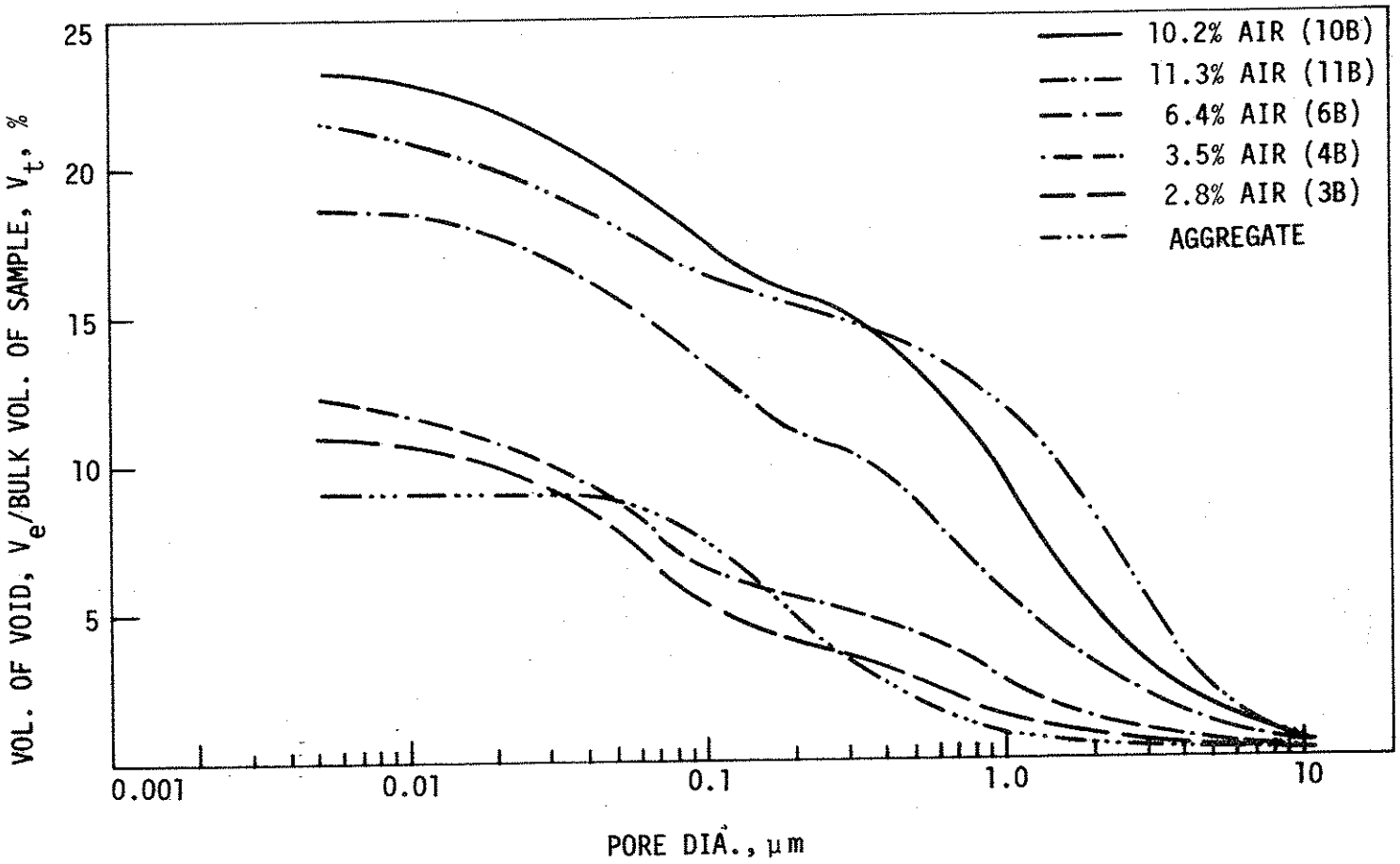

Fig. 15 Cumulative pore volume as percent of bulk volume of concrete vs pore diameter of five concretes studied.

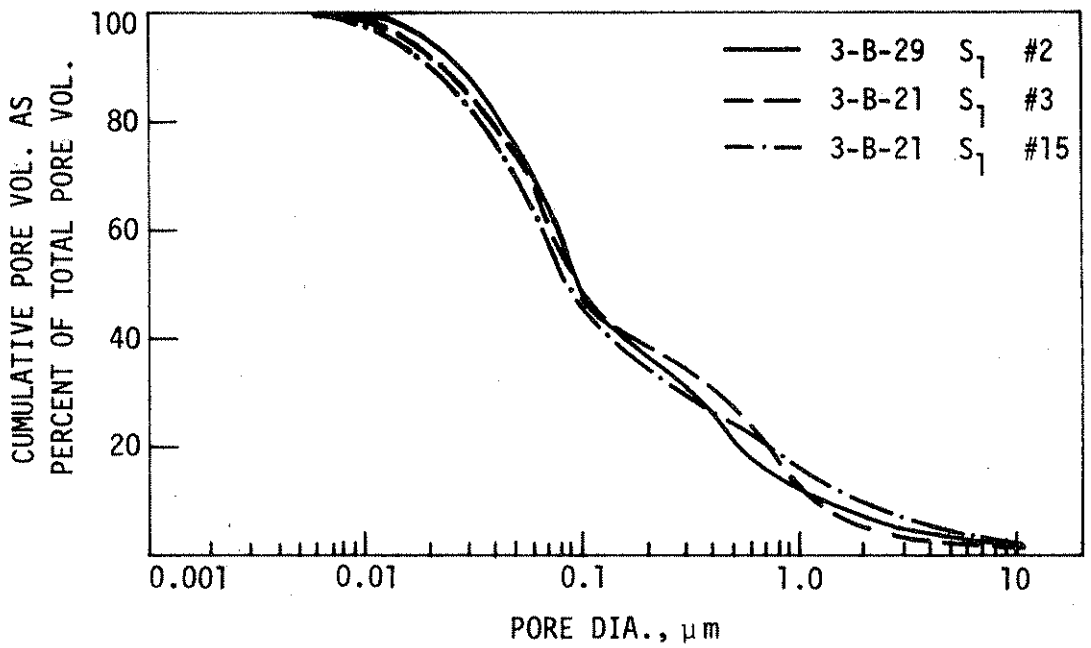

Fig. 16 Cumulative pore volume as percent of total pore volume vs pore diameter - Non-air-entrained concrete.

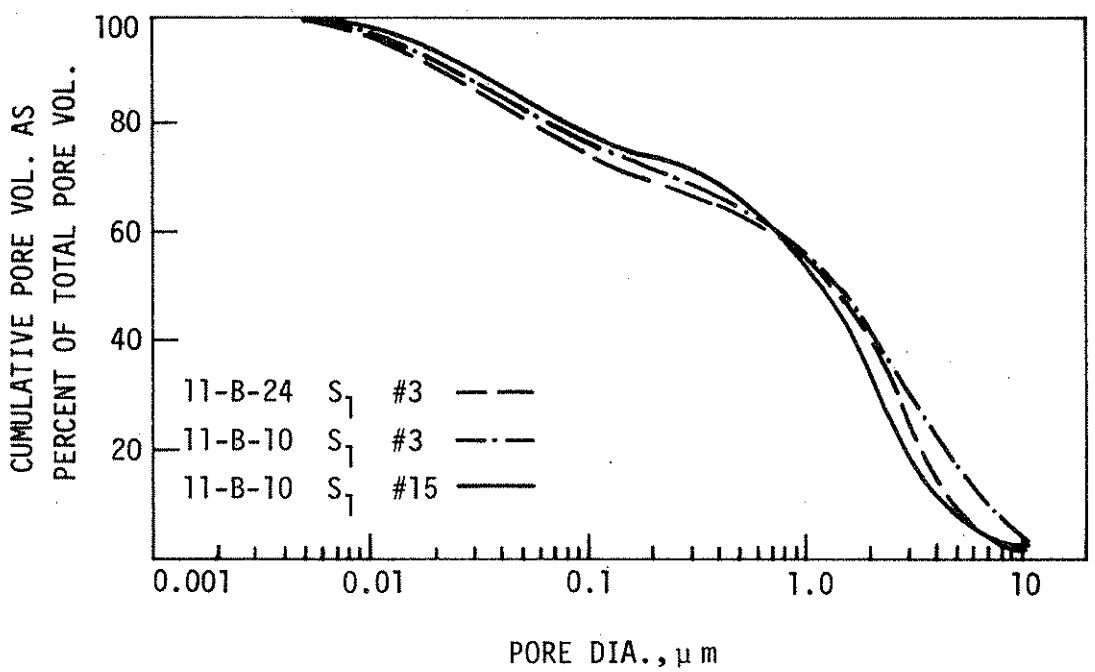

Fig. 17 Cumulative pore volume as percent of total pore volume vs pore diameter - 11.3% air.

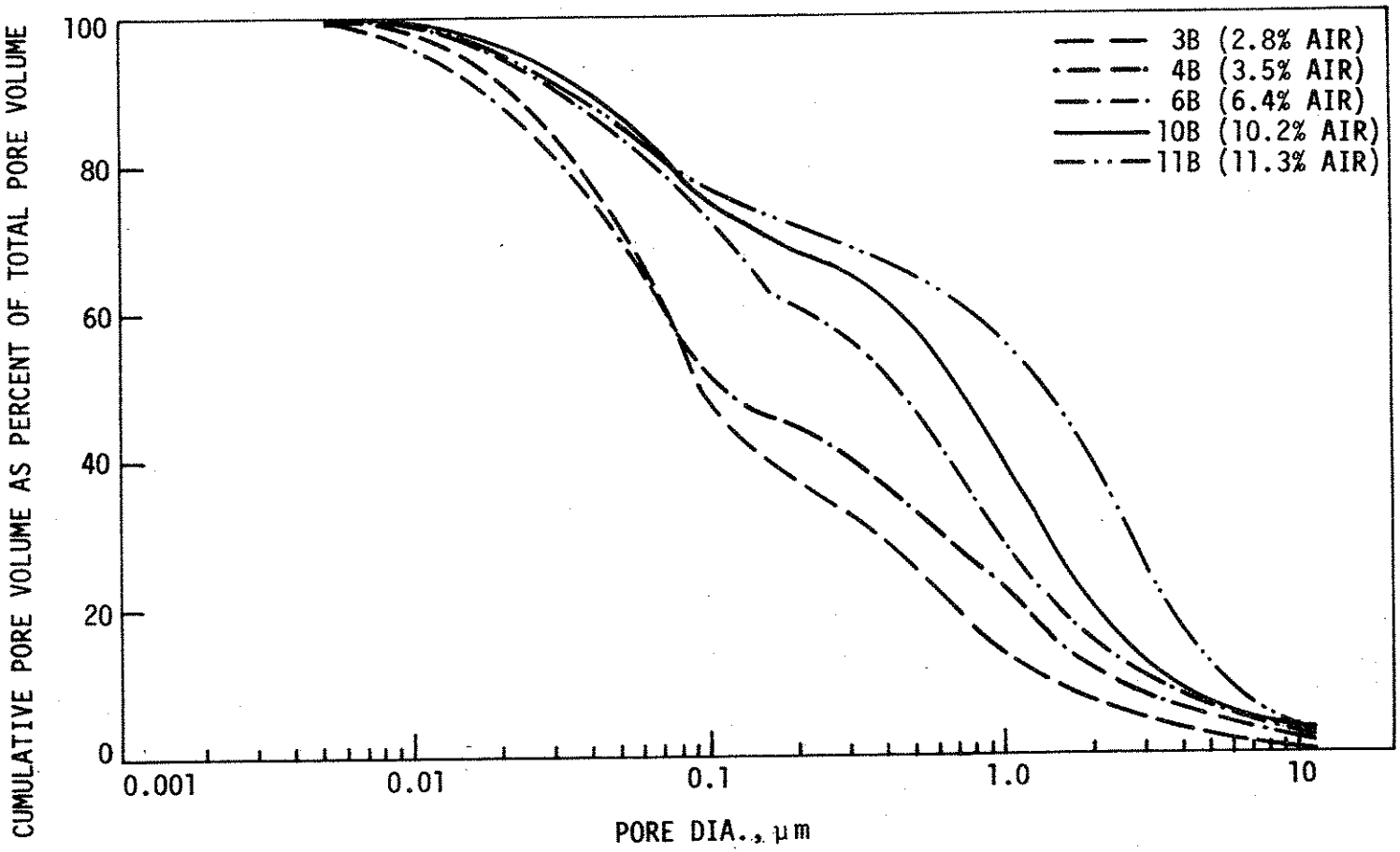

Fig. 18 Cumulative pore volume as percent of total pore volume vs pore diameter of five concretes studied.

roughly to the capillary pores.[5,47,50] This increase may also be noted in Fig. 19, in which percent of pores larger than 1.0 μm was plotted against total air content and porosity. Pore volume between 1 and 10 μm (excluding pores in aggregate) increased from 0.5% for 2.8% air (non-air-entrained) concrete to 11.0% for 11.3% air concrete. The percent pores in the 0.008 to 1 μm range remained essentially unchanged at about 11% (including aggregate pores). Although microcracks could cause some increase in porosity in the range between 1 and 10 μm, the consistent increase in pore volume in this region with increasing air content suggests that it was the direct result of air entrainment. Some evidence of these air bubbles was also observed in SEM micrographs.

4. The median pore diameter (D_{50}) also increased with total air content, from 0.1 μm at 2.8% air to 1.3 μm at 11.2% air (Fig. 20).

5. Figure 21 shows the relationship between mercury retained in the pores at atmospheric pressure as percent of volume of mercury filled at maximum pressure (40,000 psi) and percent total air (porosity). Since lower percent retention indicates pores with more or less uniform cross sections and large retention indicates pores with enlargements or constrictions (ink-bottle pores),[5] the increase in mercury retention with increase in air content indicates that the air entrainment introduces more non-uniform pores. This is also shown in the uniformity coefficient (D_{40}/D_{80}) versus air content curve (Fig. 22), higher uniformity coefficient indicating less uniform pore size distribution.

4.4. Results of Fatigue Tests

One hundred and twelve beams were subjected to flexural fatigue testing. As has been previously stated, beams of five different air contents (2.8%, 3.5%, 6.4%, 10.2%, and 11.3%) were tested.

Within each air content group, beams were tested at four different stress levels. A minimum of five beams within each of the groups were tested at each stress level. The only exception was in the first group (3.5% air), where, due to fatigue machine down time, fewer beams

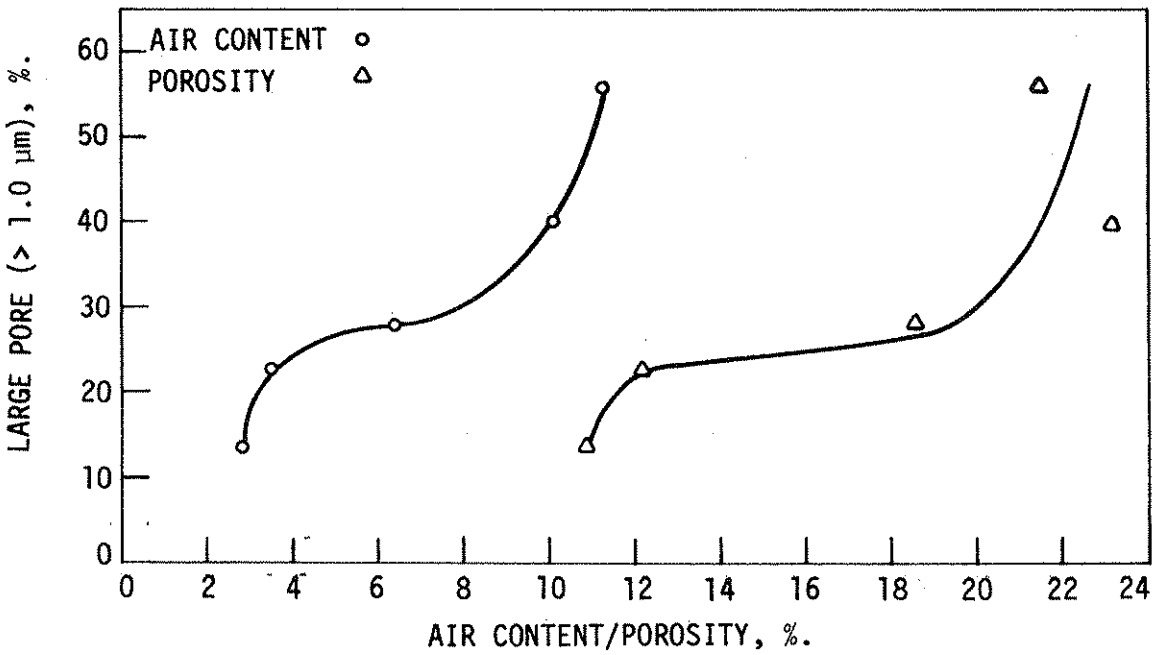

Fig. 19 Relationship between volume of large mode pores and total air content/porosity.

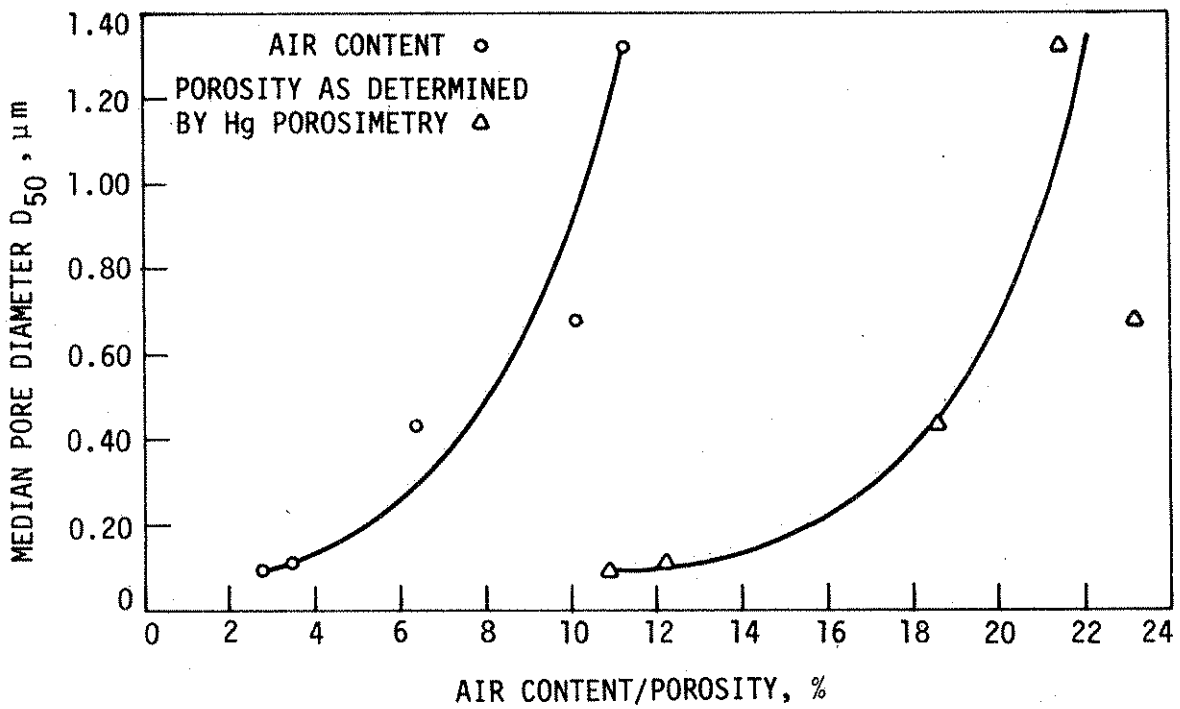

Fig. 20 Relationship between air content/porosity and median pore diameter.

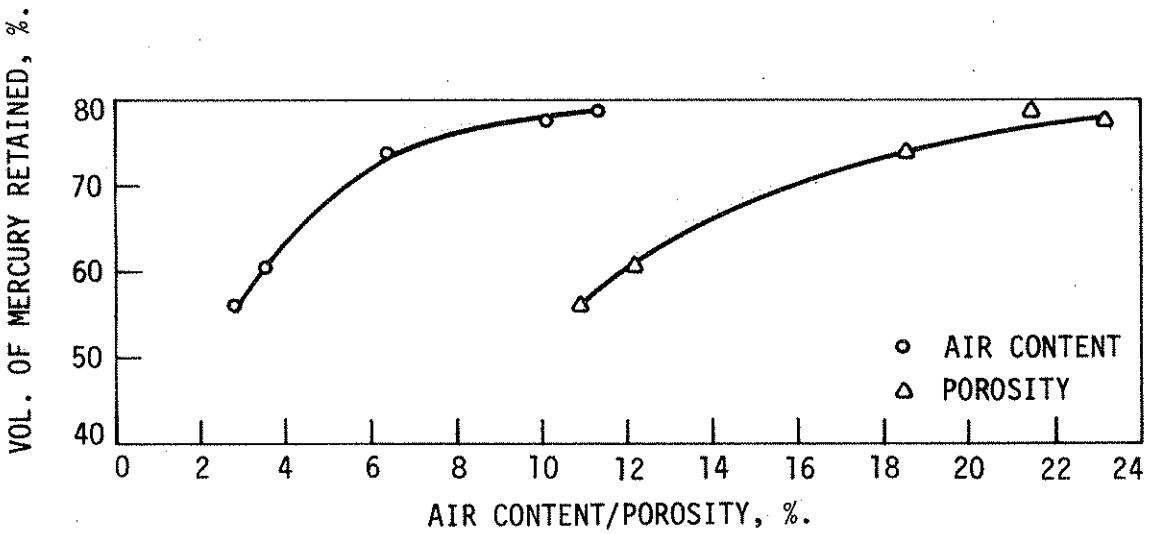

Fig. 21 Relationship between volume of mercury retained and total air content/porosity.

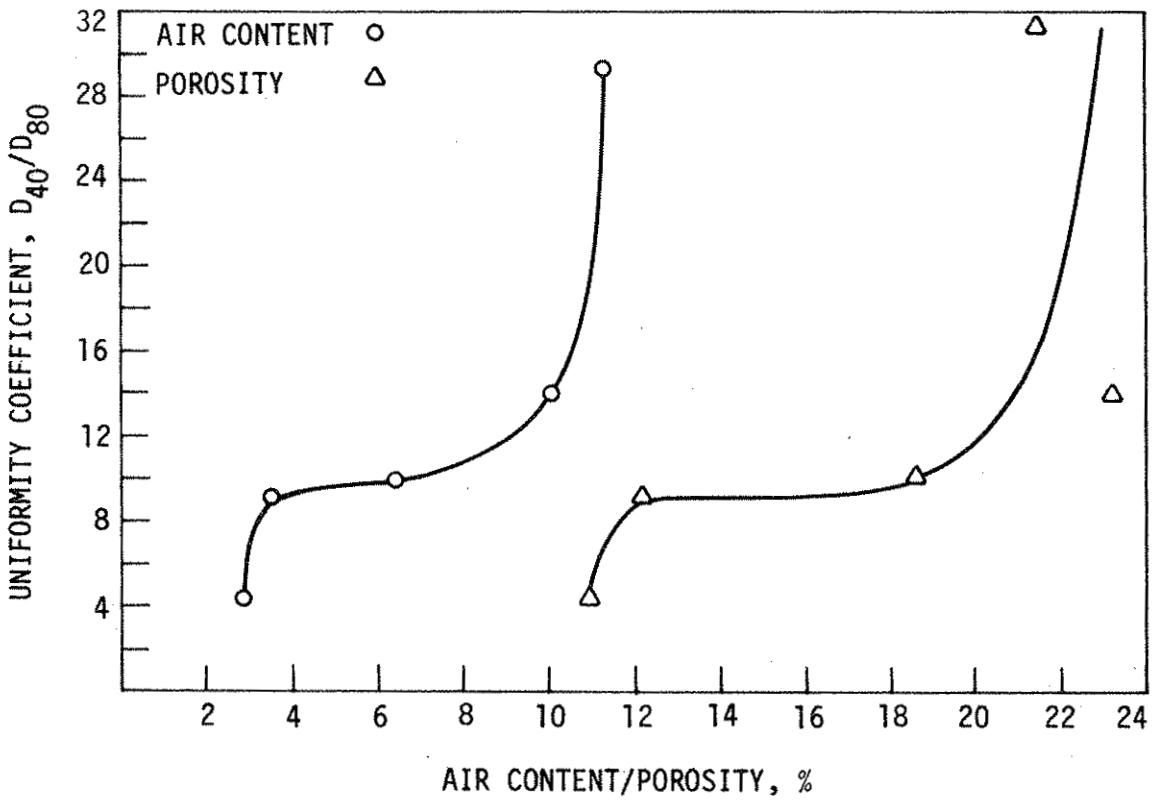

Fig. 22 Relationship between uniformity coefficient and air content/porosity.

were tested at two of the stress levels. Modulus of rupture strength, maximum load applied as a percentage of modulus of rupture, and fatigue life for each specimen are given in Tables B-1 through B-5 in Appendix B. Each specimen listed in these tables has a three-digit designation, for example, 3-B-21; the first number indicates the percent of plastic air in the concrete rounded to the nearest whole number, the letter designates the specimen as being a beam, while the second number is simply the specimen number and varies from 1 to the number of specimens cast in each batch. Specimens which did not fail are also indicated in these tables. As may be noted, specimens which did not fail were loaded a minimum of 2 million cycles. In each case the minimum stress applied was approximately 15 psi. Therefore, the beams were stressed so that the bottom fiber stress varied from essentially zero to a maximum value of 60, 70, 80, or 90% of the modulus of rupture strength. Figure 23 shows the failure faces of modulus of rupture specimens (upper section) and fatigue specimens (lower section) for three air contents: 2.8, 6.4, and 11.3%. By observing the failure surfaces, one may note that there is no visual difference between the modulus of rupture failure surface and the fatigue failure surface for each of the three air contents. However, there is a difference between the failure surfaces of the various air contents. The failure surfaces for the low air specimens exhibit predominantly failure through the coarse aggregate. Failure surfaces for the high air specimens show some failure of the aggregate; however, the main failure is between the cement paste matrix and the aggregate. Thus, it may be concluded

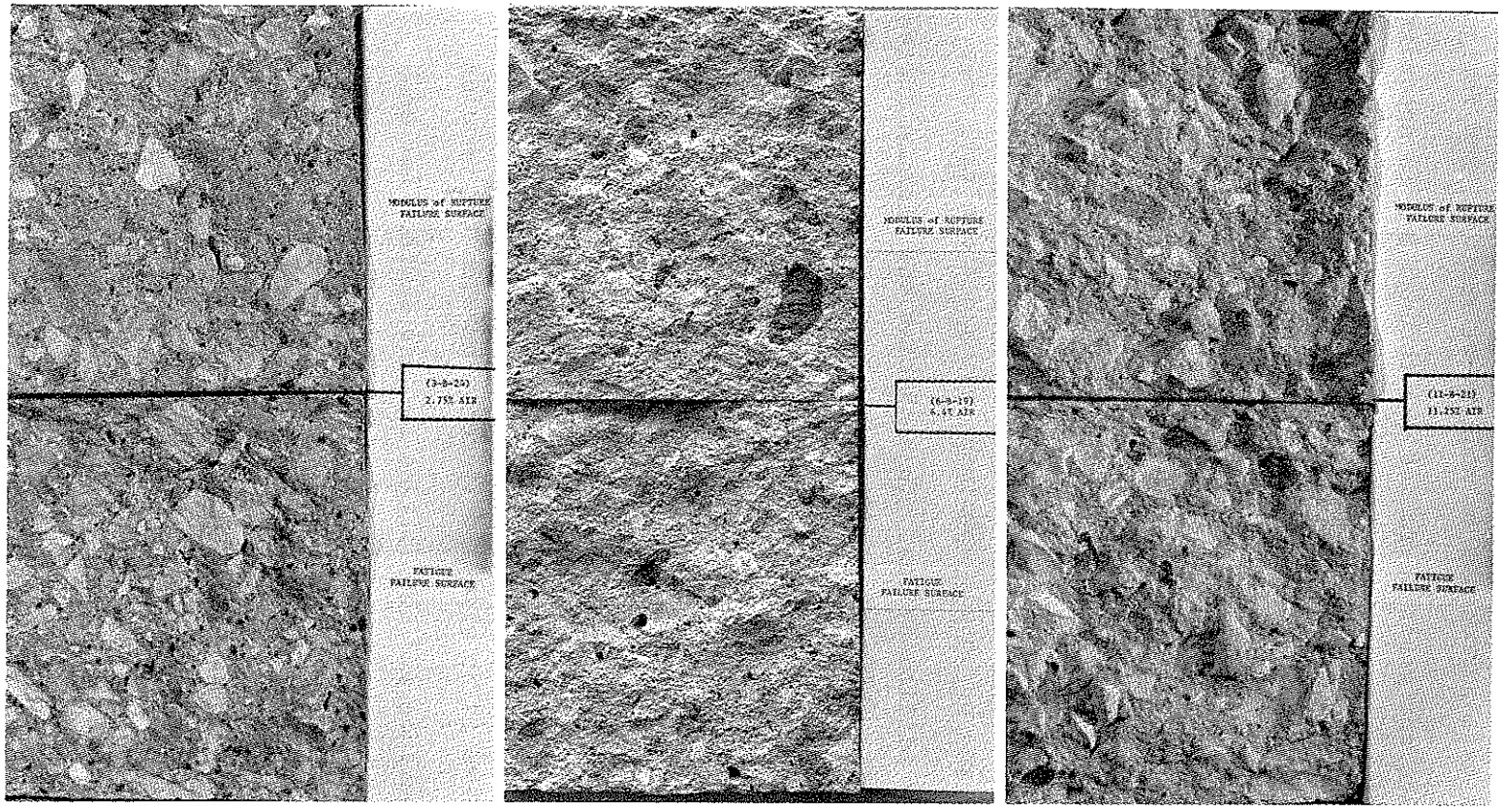

(A) (B) (C)

Fig. 23 Photographs of tested beams showing fractured faces.

that high percentages of air weaken the interlock or bond between the cement past matrix and the aggregate.

In Figs. 24 through 28 these data have been plotted on S-N curves for each of the five air contents. Each of these curves is the result of a log-log regression analysis plotted on a semi-log scale. The correlation coefficients for the curves varied from -0.90 to -0.94. Specimens that did not fail before 2 million cycles of load were assigned a fatigue life of 10 million cycles and have been indicated on the curves with small arrows.

For comparison, the curves presented in Figs. 24 through 28 are presented on a composite plot in Fig. 29. As may be seen in Fig. 29, air content has a definite effect on fatigue strength. By comparing the various curves with the 2.8% air curve, which is the natural air curve, i.e., no air-entraining agent added, one may see the decrease in fatigue strength as the air content increases. Ninety five percent confidence limits are shown for 11.3 and 2.8% air in Fig. 30. Confidence limits for the middle range air contents (3.5, 6.4, and 10.2%), although not included in this figure do exhibit a considerable amount of overlap. Confidence limits for 2.8 and 11.3% air curves overlap only slightly at the ends of the ranges. This indicates that while the precise locations of the middle range curves are probably not statistically significant, the trend of the data is statistically significant and unmistakable. Furthermore, the curves diverge at the lower stress levels. Based on these findings it can be concluded that air content has an undeniable effect on the fatigue strength of plain concrete in flexure. As air content increases, the expected fatigue life of a

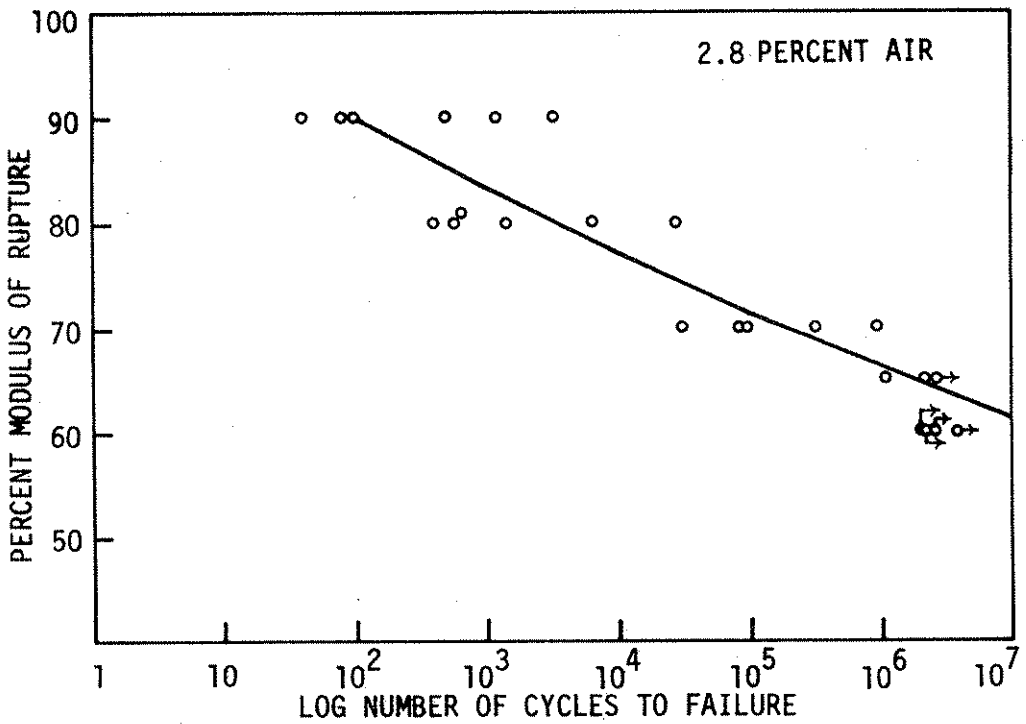

Fig. 24 S-N curve for 2.8% air concrete.

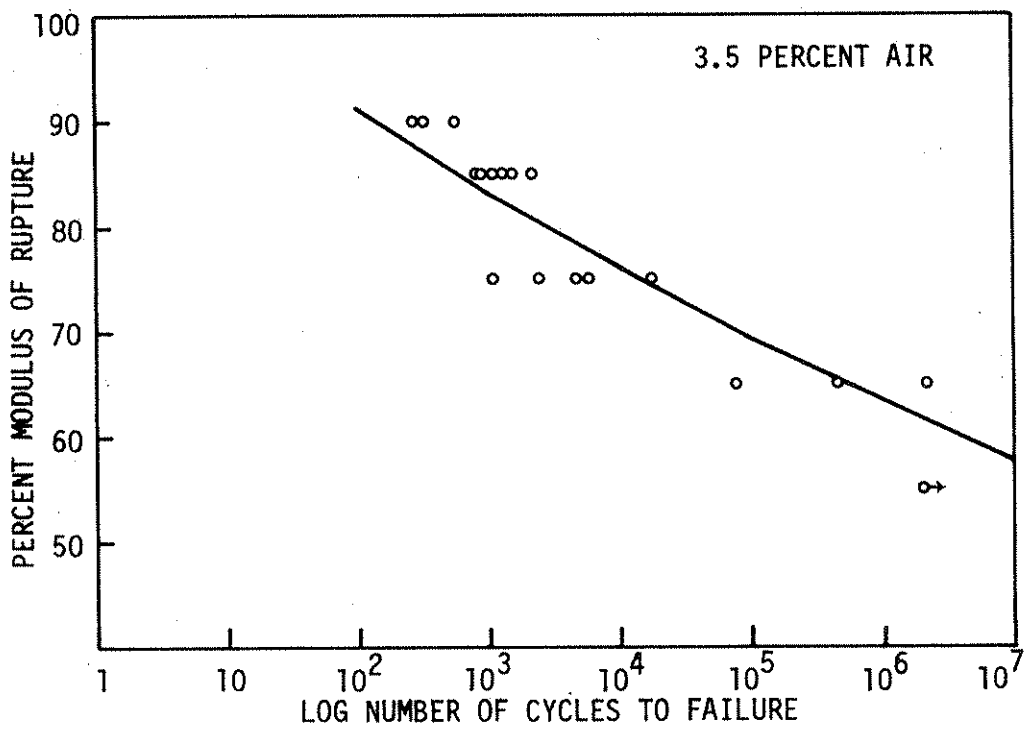

Fig. 25 S-N curve for 3.5% air concrete.

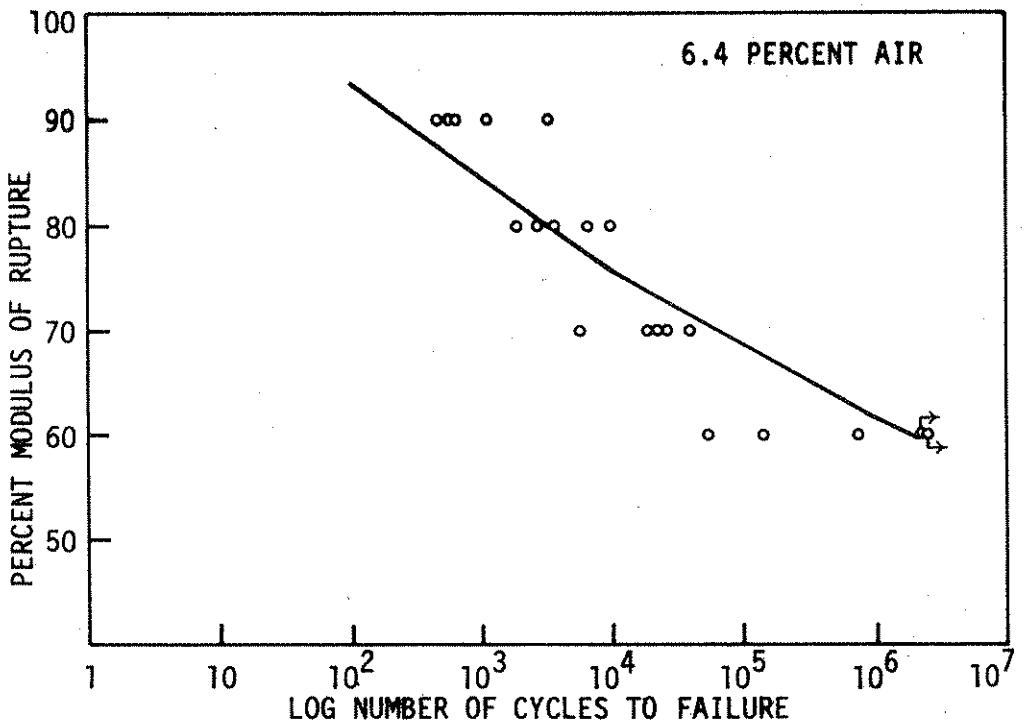

Fig. 26 S-N curve for 6.4% air concrete.

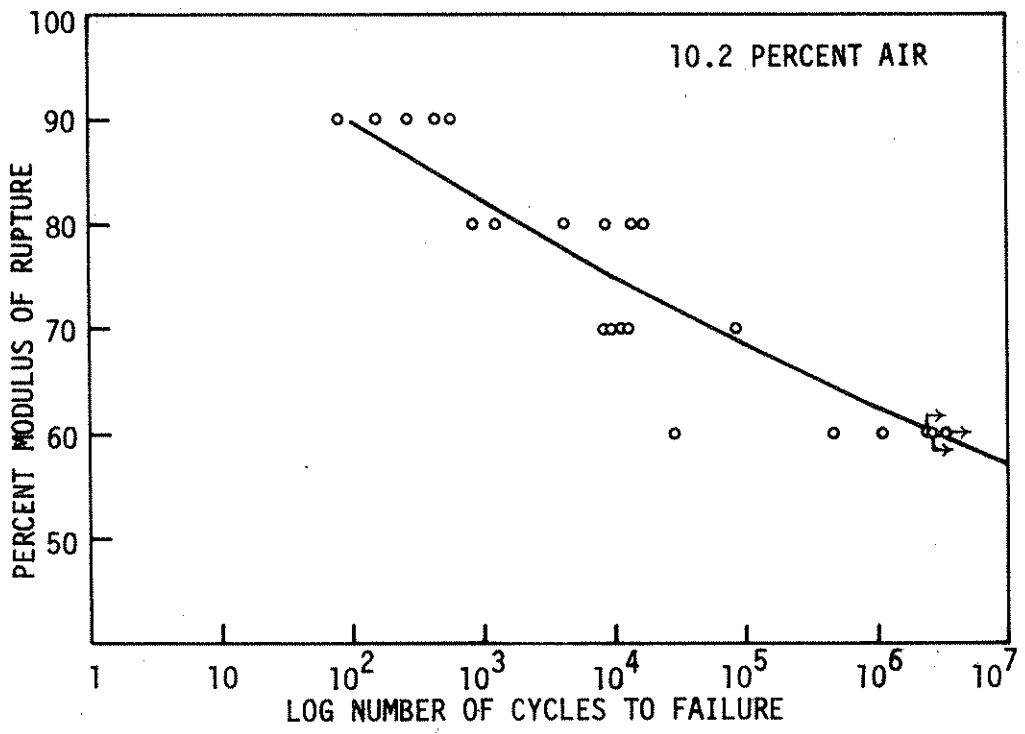

Fig. 27 S-N curve for 10.2% air concrete.

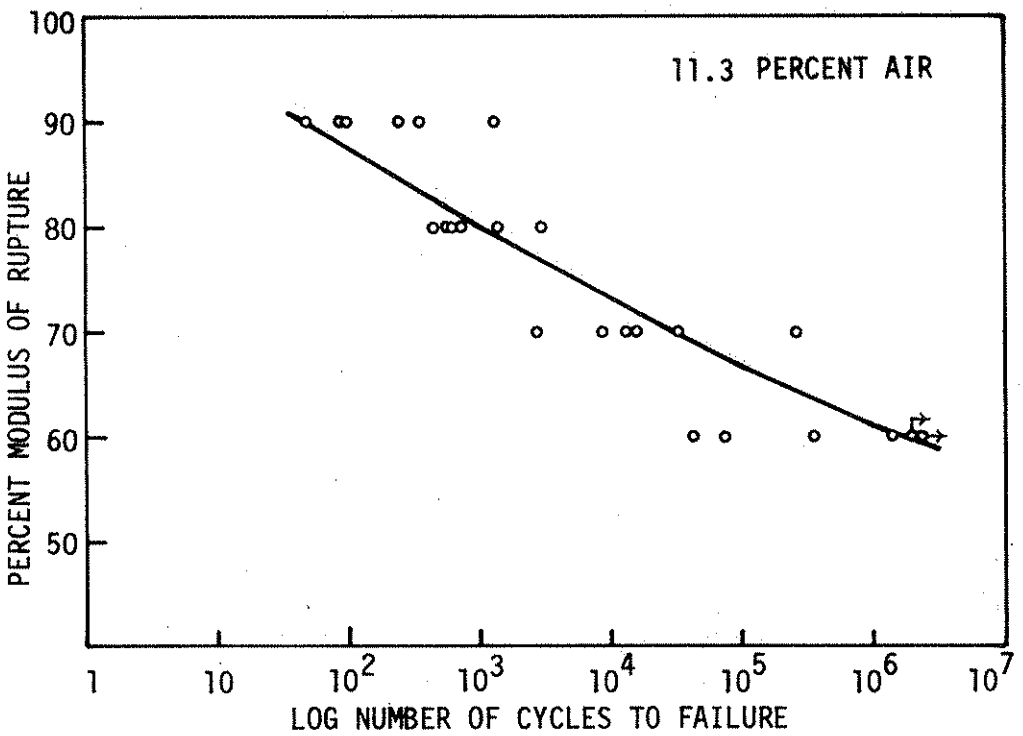

Fig. 28 S-N curve for 11.3% air concrete.

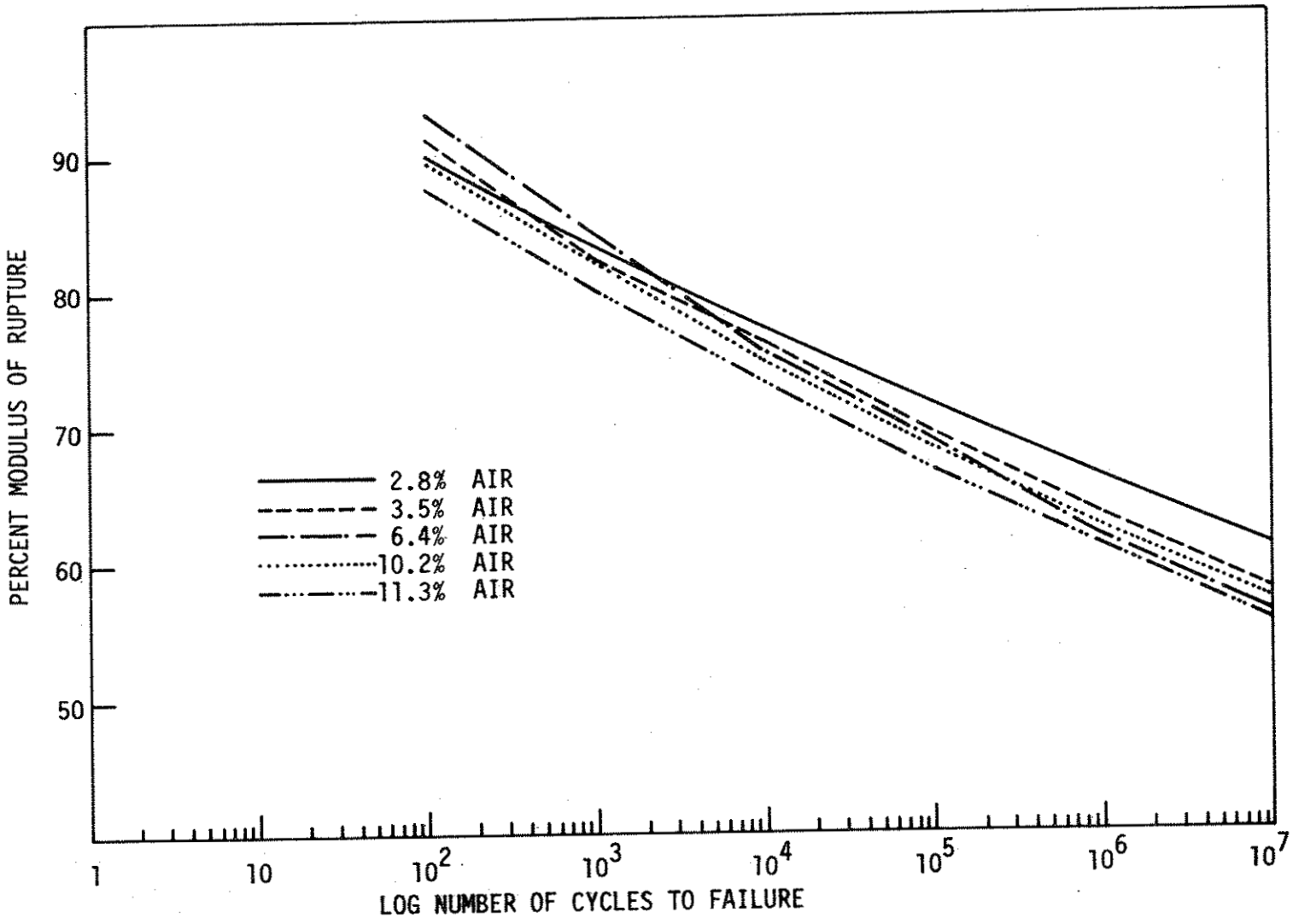

Fig. 29 Composite S-N curves for five concretes studied.

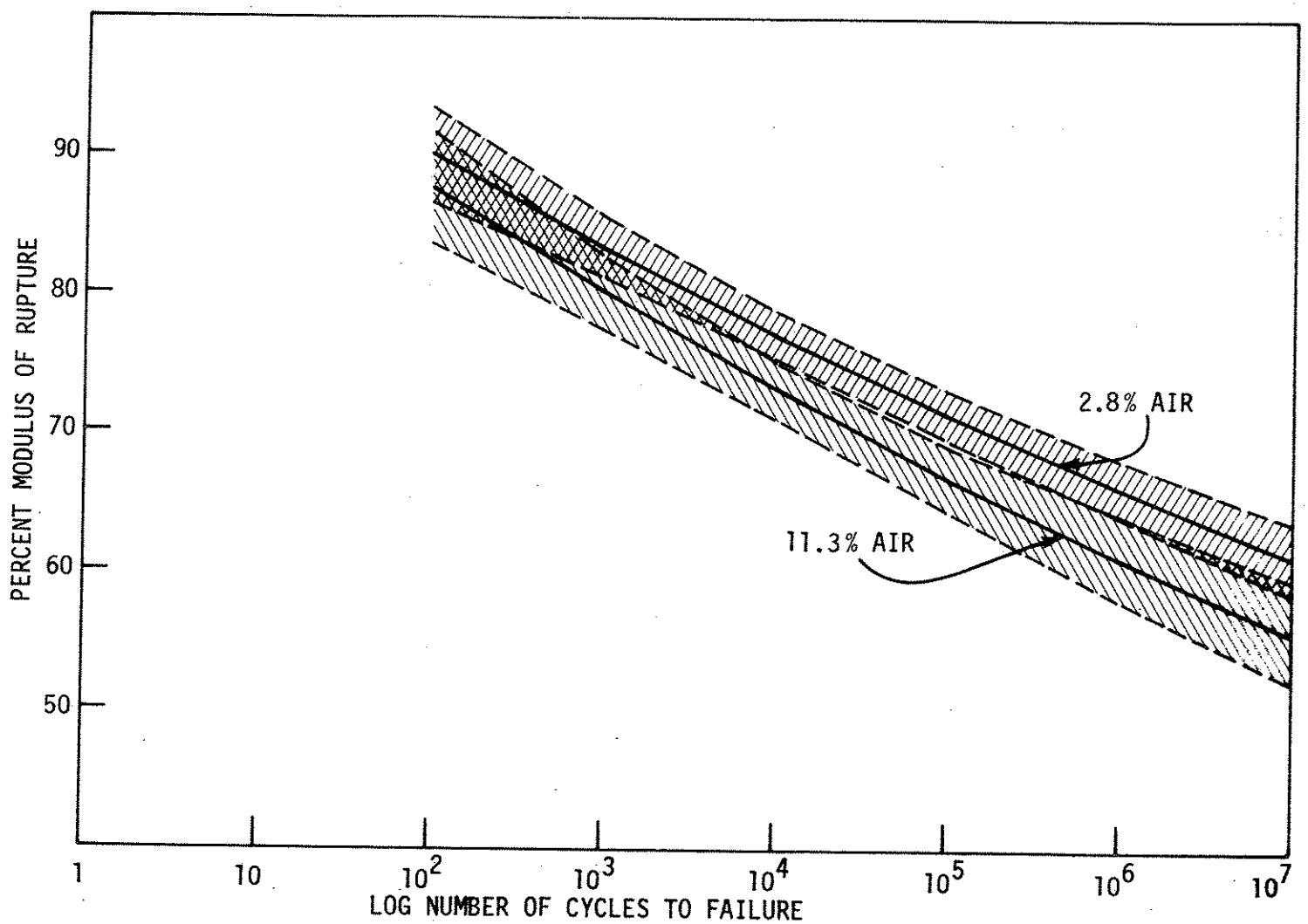

Fig. 30 Confidence limits for plain concrete with 2.8% and 11.3% air.

concrete specimen decreases. Although not obvious from the curves, due to the semi-log plot, the effect of air is more drastic at the lower stress ranges than at higher stress ranges. For instance, at the 70% stress level 11.3% air concrete would have an anticipated fatigue life of 30,000 cycles compared with 200,000 cycles for a 2.8% air concrete. At the 65% stress level, the values are 200,000 and 1,700,000 cycles, respectively. The difference in fatigue lives of the two concretes at 70% modulus of rupture is 130,000 cycles, while the difference at 65% is 1,500,000 cycles. The lower stress ranges are crucial with respect to pavement design, making this divergence of critical importance.

A modified Goodman diagram[22] for the fatigue data at one million cycles is shown in Fig. 31. Any point on a modified Goodman diagram of this type indicates a load combination that will cause a fatigue failure at one million cycles. For instance, the diagram can be used if it were desired to cycle from 60% to some maximum percentage of the modulus of rupture instead of from zero to maximum. If the minimum were set at 60%, then a specimen with 11.3% air could be loaded up to 68% and still fail at one million cycles. A 2.8% air specimen could be cycled from 60% to 73% modulus of rupture and also fail at one million load repetitions.

If tests were performed from zero to maximum load, the 11.8% and 2.8% air specimens could be subjected to 61% and 66.5% modulus of rupture, respectively, and also fail at 1 million cycles. In other words, for the same fatigue life of 1 million cycles, the low air

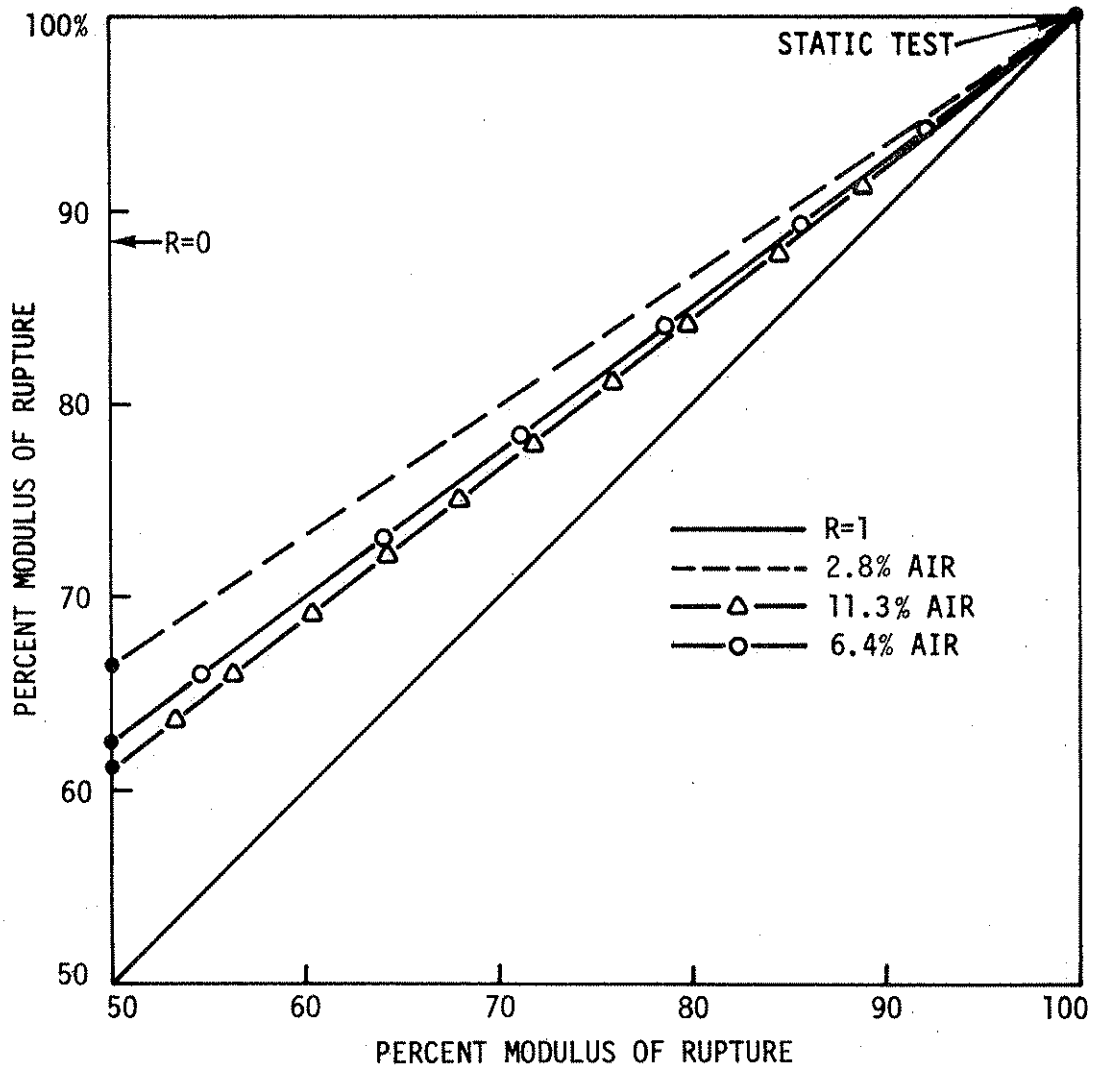

Fig. 31 Modified Goodman diagram for plain concrete with 2.8, 6.4 and 11.3% air.

concrete can withstand an additional stress equal to 5.5% of the modulus of rupture.

4.5. Treatment of Fatigue Data by Application of Fracture Mechanics

Fracture of a material occurs by extension of a pre-existing flaw. The importance of the size of the flaw depends on the fracture toughness of the material. Crack extension occurs in three stages: subcritical, critical, and running. Subcritical crack extension is slow and is measured as a length change per cycle for fatigue. At critical crack extension there is a transition from a slowly propagating crack to a rapidly running crack. Running crack extension corresponds to fracture of the material. In order to understand the fracture behavior of a material the transition point from subcritical to critical crack extension must be quantified.

Fracture of concrete can occur by fracture of the cement paste, fracture of the aggregate, failure of the bond between cement paste and aggregate, or any combination of these. For this reason concrete differs slightly from the ideal crack extension behavior. "Two types of crack growth are present in concrete: an initial stage in which the rate of release of strain energy with slow crack extension is so low that any sudden increase in energy requirement, such as encountering an aggregate, will stabilize the propagating crack; and a final stage where the energy release rate with rapid crack propagation is of such magnitude that any energy demand encountered will be supplied so that an unstable situation results."[34] The transition between these two

stages is a function of the critical stress intensity factor, K_c. The smaller the K_c, the smaller crack length is required for failure in fracture. In general, the stress intensity factor (K) can be expressed as:

$$K = JC\ (A)^{\frac{1}{2}}$$

where J = stress, A = crack length, and C is some constant dependent on the geometry of the material.

Brown and Srawley[8] developed the following expression for K, for a single-edge-cracked specimen subjected to pure bending:

$$K = Y\ \frac{6Ma^{\frac{1}{2}}}{Bw^2}$$

where $Y = 1.99 - 2.47\ (a/w) + 12.97\ (a/w)^2 - 23.17\ (a/w)^3 + 24.80\ (a/w)^4$, a is the flaw depth, w is specimen depth, M is applied bending moment, and B is specimen width.

Rolfe and Barsom[42] presented equations for K for various other conditions.

If stress (or moment above) is held constant, then the only variable for a constant geometry section is the crack length a. The critical stress intensity factor (K_c) then corresponds to some critical crack length a_c. When this critical crack length is reached, the transition between slow and rapid crack propagation will occur.

Fatigue behavior of concrete can then be thought of as a phenomenon involving the growth of microscopic flaws. When the length of one of these flaws reaches the critical value a_c, failure will occur. The fatigue behavior is directly affected by the critical stress intensity factor, K_c: As K_c goes up, a_c also increases. The

importance of this statement with respect to understanding the fatigue behavior of air-entrained concrete can be fully understood in light of the findings of Naus and Lott.[34] Naus and Lott found that K_c decreased by 8.2% when the air content in concrete was increased from 2.0 to 12.0%.

This finding indicates a decrease in the critical crack length a_c, with increasing air content. If it can be assumed that microcracking occurs at similar rates for varying air contents, then a decrease in a_c will mean a fewer number of load (stress) repetitions will be required to effect a fracture or fatigue failure. In other words, as air content increases and K_c (and a_c) decreases, fatigue life would be expected to decrease.

This theoretical approach is in agreement with the experimental findings of this investigation. The flexural fatigue life of concrete was found to decrease as the amount of air increased between the limits of 2.8 and 11.3%.

4.6. Implications in Concrete Pavement Design

The results of two research projects carried out in the early 1920's at Purdue and the Illinois Department of Highways[11,37] provided basic data for the 1933 PCA fatigue curve shown in Fig. 32.[13] This curve was used in conjunction with Minor's theory[32] to evaluate the accumulated fatigue effects of all anticipated load applications, to prevent slab cracking, and to evaluate the design adequacy of a concrete slab thickness for streets, highways, and airfields. Minor's

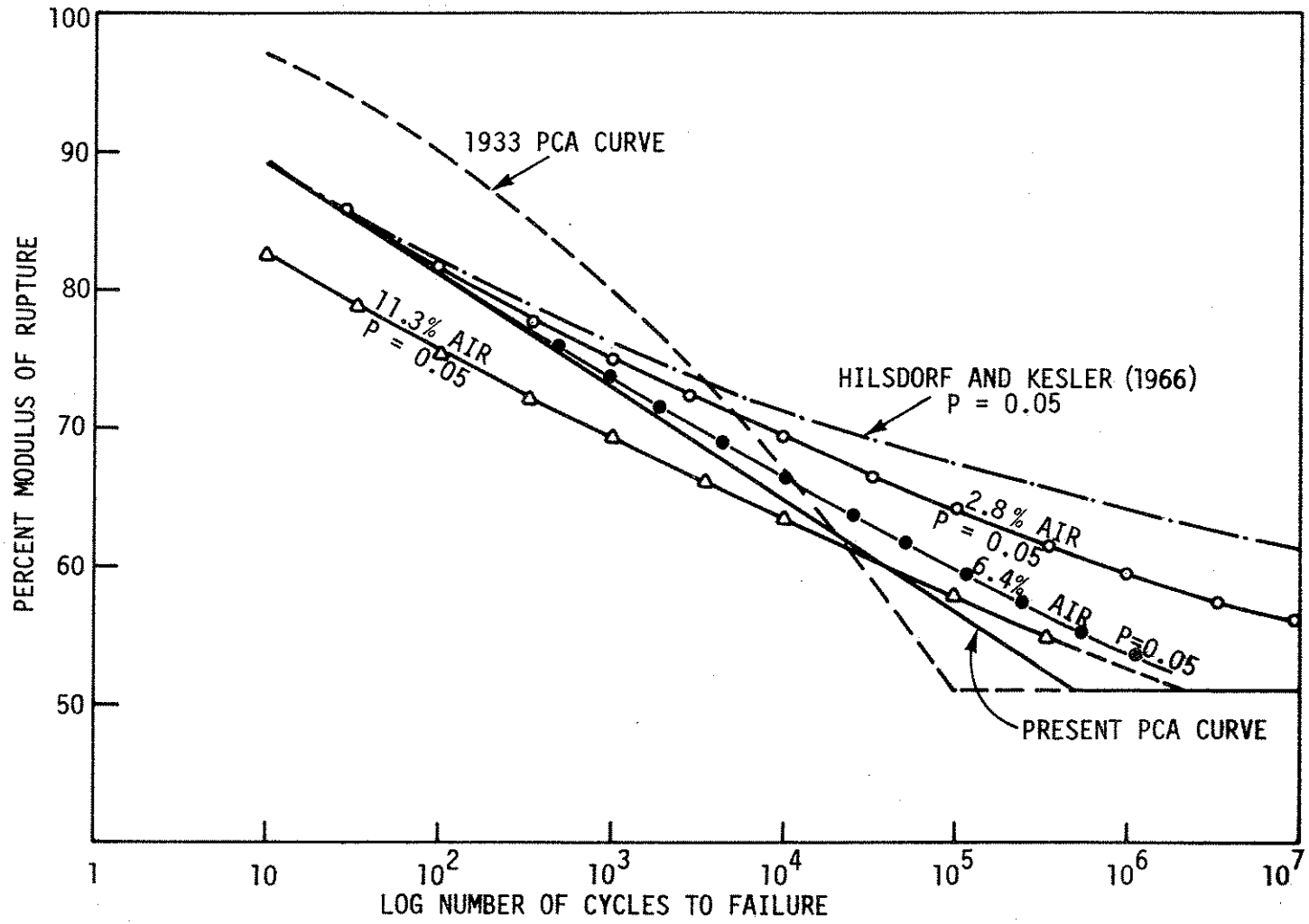

Fig. 32 Pavement fatigue (S-N) design curves.

theory applies to stress repetitions above the endurance limit and postulates that fatigue strength not used by repetitions at one stress level is available for repetitions at other stress levels; Minor's theory is often referred to as the cumulative damage theory. Due in part to work done in the 1960's by Hilsdorf and Kesler[18] and, in part to results of several test roads, the 1933 PCA fatigue curve was replaced by the present 1966 curve.

The fatigue curve which resulted from the work by Hilsdorf and Kesler is shown in Fig. 32. This curve represents a constant probability of 0.05, which means that for 100 fatigue tests not more than five would show fatigue strengths below the curve. Calculations of pavement thickness with the Hilsdorf and Kesler curve gave usable results, and their curve was considered for replacement of the 1933 PCA curve. However, due to the limitations of the Hilsdorf and Kesler investigation, evidence from several test roads, and performance of normally constructed pavements subject to normal mixed traffic, the present PCA curve was adopted for thickness design.

Results of the current investigation are also shown in Fig. 32 for non-air-entrained (2.8%), medium range air (6.4%), and high air-entrained concrete (11.3%). These curves also represent a constant probability of 0.05 and can therefore be compared directly with the work of Hilsdorf and Kesler and the two PCA fatigue curves.

It should be kept in mind that the curve presented by Hilsdorf and Kesler is the result of varying stress fatigue, while the findings of this investigation are the result of constant stress fatigue testing.

The present PCA fatigue curve is conservative with respect to Hilsdorf and Kesler air curve as well as the 2.8% air curve of this investigation. When the effect of high air content is considered, the PCA curve is not conservative in the higher stress ranges. The location of the 11.3% air curve indicates that a pavement designed by current PCA procedures and containing this much air could fail prematurely. This illustrates most dramatically the effect of air content on current pavement design procedures.

To further illustrate the effect of air content, pavement designs were performed using the Iowa DOT Pavement Design Procedure[15] with the fatigue curves from this investigation as well as the standard PCA 1933 and 1966 fatigue curves. The results are compared in terms of both fatigue consumption for a given slab thickness and the slab thickness required to ensure against fatigue failure. The same design traffic data and subgrade k values were used in all cases. The fatigue curves that were used are those shown in Fig. 32. The distribution of axle loads during the design life corresponds to Design Example Number 2 of reference 45. The design calculations are presented in Appendix C. The effect of air content on the modulus of rupture was taken into account. Values of modulus of rupture used were 500 psi for 11.3% air, 700 psi for 2.8% air, and 600 psi for 6.4% air, which correspond to the 600 psi used for the PCA design calculations. The results of the thickness design calculations are presented in Table 3.

For the given subgrade, traffic, and modulus of rupture, based on Iowa D.O.T. design methods, a pavement thickness of 9.5 in. is required. Using this thickness as a basis for comparison, the current

Table 3. Comparison of pavement design procedures.

	Design Procedure				
	PCA		I.S.U.		
	Iowa DOT (Current PCA)	1933 PCA	2.8% Air Curve	6.4% Air Curve	11.3% Air Curve
Assumed Modulus of Rupture, psi	600	600	700	600	500
% Fatigue Life used in a 9.5 in. Pavement	75.1	196.9	None	16.9	3322.6
Pavement Thickness Required for Less Than 125% Fatigue Life Consumption, in.	9.5	10.0	7.5	9.0	10.5

D.O.T. procedure arrives at a value of 75.1% of the available fatigue life used. The 1933 PCA fatigue curve results in a fatigue life consumption of 196.9%. With 2.8% air and using the I.S.U. fatigue curve, none of the fatigue life is used. At 6.4% air, 16.9% of the fatigue life is used, and at 11.3% air, 3322.6% of the fatigue life would be used.

A more meaningful comparison can be made by calculating the respective pavement thickness required when each of the fatigue curves is used. The current PCA fatigue curve will require a thickness of 9.5 in. The 1933 curve would require 10.0 in. If the fatigue curve for an air content of 2.8% is used, the thickness required could be held down to 7.5 in. A 6.4% air pavement would require a thickness of 9.0 in. However, if the fatigue curve for an 11.3% air concrete were used, a 10.5-in. pavement would be required. This again illustrates the effect of air content on current pavement design practices.

It should be noted that the air contents used for the previous comparison are out of the range of normal design for concrete mixes. This, however, does not alter the basic finding of this investigation, that air content does indeed affect the fatigue life of plain concrete in flexure and should be considered for optimum design of concrete pavements.

5. SUMMARY AND CONCLUSIONS

The need for fatigue strength data in the design of concrete highway and airfield pavements has been known for years. Practically all rigid pavement design procedures used today make use of the fatigue life of concrete. The fatigue curves presently used were last revised in 1966 and do not take into account the effects of entrained air. Thus, this study investigated the effectsof air on fatigue strength of plain concrete. All other variables (water-cement ratio, aggregate type, cement type, etc.) were held constant.

The previous text presents the results of the study on the fatigue behavior of plain concrete of various air contents. Tests were conducted on five batches of concrete with air contents of 2.8, 3.5, 6.4, 10.2, and 11.3%. Fatigue specimens consisted of 6 in. x 6 in. beams subjected to flexural loading under a zero to maximum load cycle. Under such conditions the bottom fiber of the beam was subjected to zero to tension stress cycles. The maximum bottom fiber stress for a specific test in most cases was 60, 70, 80, or 90% of the static modulus of rupture. Concrete for all batches was mixed and poured in the laboratory. Test specimens were stored submerged in water until testing which took place at a specimen age of 28 to 56 days.

Tests were conducted using an Instron Corporation model 1211 dynamic cycler fitted with a one-third point loading frame identical to the one used in the modulus of rupture test. One hundred and twelve fatigue tests were conducted. Results of these tests are presented in both tabular and graphic form.

S-N diagrams show a significant reduction in fatigue life as the air content of concrete increases. This reduction is further illustrated when S-N curves with 95% confidence limits for a point are used for pavement design. Using the I.S.U. fatigue curves, a pavement containing 2.8% air would require a design thickness of 7.5 in., while a pavement containing 6.4% air would require a design thickness of 9.0 in.

The main fatigue test program was supplemented by additional investigations. The compressive strength, modulus of rupture, modulus of elasticity, and unit weight were determined for each batch. Plastic air content determinations were compared with hardened air contents determined by the linear traverse and high pressure air meter methods. Scanning electron microscope photographs were taken at various magnifications and various air contents to determine characteristics of the air void system. A mercury penetration porosimeter was used to characterize the void properties of the concrete at the various air contents.

As a result of the various tests performed in this study the following conclusions were reached:

1. The fatigue behavior of plain concrete in flexure is affected by the air content of the concrete. Fatigue strength decreases as air content increases. Fatigue curves obtained from this study (Figs. 29 and 32) provide a basis for an improved rigid pavement design for pavements in which air-entrained concrete is used. Pavements designed using the high air and low air fatigue curves developed in this study resulted in a difference in thickness of several inches.

2. The linear traverse and high pressure air determination methods are reliable means of ascertaining the air content of hardened concrete and can be used to determine the original plastic concrete air content by mathematical means.

3. The modulus of rupture, compressive strength, modulus of elasticity, and unit weight of concrete all decrease as the air content of the concrete increases.

4. As the air content rises the failure of concrete subjected to fatigue occurs increasingly at the aggregate-cement paste interface. The fatigue failure surface is, however, identical, on a macroscopic level, to the modulus of rupture (static) failure surface.

5. Although it has been generally suggested that entrained air voids are between 1 and 0.005 mm in diameter and spherical in shape, and that entrapped air bubbles are greater than 1 mm in diameter and irregular in shape, the SEM micrographs made in this study showed that the two kinds of voids cannot be distinguished by either size or shape.

6. Air entrainment had essentially no effect on pores of capillary/gel size (less than 1 μm). However, mercury porosimetry data showed that at higher air entrainment, increased air resulted in more pores in size of 1 to 10 μm range, between that of conventional concept of entrained air and capillary pores. Also, increasing air content increased the median pore diameter of the micropores as well as the non-uniformity of pore system.

6. RECOMMENDED FUTURE STUDIES

The present study has clearly shown that air content does have an effect on fatigue concrete in flexure. In view of these findings the following areas of concrete fatigue in flexure should be pursued:

- Effects of varied W/C ratio
- Effects of different aggregate types
- Surface treatments and other approaches to increase fatigue life (high density surface, polymer, sulfur penetration, etc.)
- Development of comprehensive rigid pavement design curves applicable for concretes of commonly used combinations of air content, water-cement ratio, aggregate type, etc.

7. REFERENCES

1. AASHTO Interim Guide for Design of Pavement Structures, 1962.

2. A Guide to the Structural Design of Pavements for New Roads, Road Research Laboratory, Road Note 29, 1970.

3. Air Entrained Concrete. Washington, D.C., Highway Research Board, Bulletin 70, 1953.

4. Antrim, J. C. and J. F. McLaughlin. "Fatigue Study of Air Entrained Concrete." American Concrete Institute Journal, Proceedings, Vol. 55, May 1959, pp. 1173-1182.

5. Auskern, A. and W. Horn. "Capillary Porosity in Hardened Cement Paste." Journal of Testing and Evaluation, Vol. 1, No. 1., 1973, pp. 74-79.

6. Bennett, E. W. "Fatigue in Concrete." Concrete (Chicago), May 1974, pp. 43-45.

7. Brown, L. S. and C. U. Pierson. "Linear Traverse Technique for Measurement of Air in Hardened Concrete." American Concrete Institute Journal, Proceedings, Vol. 47, 1950, pp. 117-123.

8. Brown, W. F. and J. E. Srawley. "Plain Strain Crack Toughness Testing of High Strength Metallic Materials." America Society of Testing and Materials, STP No. 410, 1966, pp. 13-14.

9. Carey, W. N. and P. E. Irick. "Relationships of AASHO Road Test Pavement Performance to Design and Load Factors." Highway Research Board, Special Report No. 73, 1962, p. 259.

10. Causes, Mechanism, and Control of Cracking in Concrete. Detroit, Michigan, American Concrete Institute, Publication SP-20, 1968.

11. Clemmer, H. F. "Fatigue of Concrete." Proceedings, American Society of Testing and Materials, Vol. 22, Part II, 1922, pp. 409-419.

12. Concrete and Mineral Aggregates. Philadelphia, Pa., American Society for Testing and Materials: Annual Book of Standards, Part 10, 1973.

13. Fordyce, P. and W. A. Yrjanson. "Modern Techniques for Thickness Design of Concrete Pavements." American Society of Civil Engineers Annual Meeting and National Meeting on Structural Engineering, 1968 (also available from Portland Cement Association).

14. Gregg, L. E. Experiments with Air Entrainment in Cement Concrete. Lexington, Kentucky, Kentucky Department of Highways, Bulletin No. 5, September 1947.

15. Guide for Primary and Interstate Road Pavement Design, Iowa Department of Transportation, 1976.

16. Hatt, W. K. "Fatigue of Concrete." Proceedings, Highway Research Board, Vol. 4, 1924, pp. 47-60.

17. Hawkins, N. M., A. N. Wyss and A. H. Mattock. "Fracture Analysis of Cracking in Concrete Beams." ASCE Journal of the Structural Division, May 1977, pp. 1015-1030.

18. Hilsdorf, H. K. and C. E. Kesler. "Fatigue Strength of Concrete Under Varying Flexural Stresses." American Concrete Institute Journal, Proceedings, Vol. 63, No. 10, October 1966, pp. 1059-1075.

19. Hollen, G. W. and M. E. Prior. "Factors Influencing Proportioning of Air Entrained Concrete." American Concrete Institute, Publication SP-46, 1974.

20. Hudson, W. R. and B. F. McCullough. "An Extension of Rigid Pavement Design Methods." Highway Research Record, No. 60, 1964, pp. 1-14.

21. Kesler, C. E., "Effect of Speed of Testing on Flexural Fatigue Strength of Plain Concrete." Proceedings, Highway Research Board, Vol. 32, 1953, pp. 251-258.

22. Kesler, C. E. Significance of Tests and Properties of Concrete-Making Materials. American Society of Testing and Materials: Special Technical Publication 169A, 1966, pp. 144-159.

23. Kosteas, D. "Effect of the Number of Samples on the Statistical and Regression Analysis of Fatigue Tests." Aluminium, Vol. 50, No. 2, 1974, pp. 165-170.

24. Lauer, K. R. and F. O. Slate. "Autogenous Healing of Cement Paste." American Concrete Institute Journal, Proceedings, Vol. 52, June 1956, pp. 1083-1098.

25. Lerch, W. Basic Principals of Air Entrained Concrete. Portland Cement Association, 1953.

26. Lindsay, J. D., "Illinois Develops High Pressure Air Meter for Determining Air-Content of Hardened Concrete." Proceedings, Highway Research Board, Vol. 35, 1956, pp. 424-435.

27. McCall, J. T. "Probability of Fatigue Failure of Plain Concrete." American Concrete Institute Journal, Proceedings, Vol. 55, August 1958, pp. 233-244.

28. Mielenz, R. C., V. E. Wolkodoff, J. E. Backstrom and H. L. Flack. "Origin, Evolution, and Effects of the Air Void System in Concrete. Part I - Entrained Air in Unhardened Concrete." American Concrete Institute Journal, Proceedings, Vol. 55, July 1958, pp. 95-122.

29. Mielenz, R. C., V. E. Wolkodoff, J. E. Backstrom and H. L. Flack. "Origin, Evolution, and Effects of the Air Void System in Concrete. Part 2 - Influence of Type and Amount of Air-Entraining Agent." American Concrete Institute Journal, Proceedings, Vol. 55, August 1958, pp. 261-283.

30. Mielenz, R. C., V. E. Wolkodoff, J. E. Backstrom and H. L. Flack. "Origin, Evolution, and Effects of the Air Void System in Concrete. Part 3 - Influence of Water-Cement Ratio and Compaction." American Concrete Institute Journal, Proceedings, Vol. 55, September 1958, pp. 359-376.

31. Mielenz, R. C., V. E. Wolkodoff, J. E. Backstrom and H. L. Flack. "Origin, Evolution, and Effects of the Air Void System in Concrete. Part 4 - The Air Void System in Job Concrete." American Concrete Institute Journal, Proceedings, Vol. 55, October 1958, pp. 507-518.

32. Miner, M. A. "Cumulative Damage in Fatigue." Transactions of the ASME, Vol. 67, 1945, pp. A159-A164.

33. Murdock, J. W. and C. E. Kesler. "Effect of Range of Stress on Fatigue Strength of Plain Concrete Beams." American Concrete Institute Journal, Proceedings, Vol. 55, August 1958, pp. 221-232.

34. Naus, D. and J. Lott, Fracture Toughness of Portland Cement Concretes. Urbana, Illinois, University of Illinois, T & AM Report No. 314, 1968.

35. Neville, A. M. Properties of Concrete. New York, John Wiley and Sons, Inc., 1973.

36. Nordby, G. M. "Fatigue of Concrete - A Review of Research." American Concrete Institute Journal, Proceedings, Vol. 55, August 1958, pp. 191-220.

37. Older, C. "Highway Research in Illinois," Transactions, American Society of Civil Engineers, Vol. 87, 1924, pp. 1180-1222.

38. Raithby, K. D. and J. W. Galloway, "Effects of Moisture Condition, Age, and Rate of Loading on Fatigue of Plain Concrete." American Concrete Institute, Publication SP-41, 1974, pp. 15-34.

39. Ray, G. K., E. G. Robbins and R. G. Packard. "Concrete Pavement Design Today." Proceedings of the American Society of Civil Engineers Conference on Pavement Design for Practicing Engineers, Atlanta, Ga., 1975, pp. 1-2.

40. Ray, G. K. "History and Development of Concrete Pavement Design." ASCE Journal of the Highway Division, Vol. 90, 1964, p. 79.

41. Reidenouer, D. R. and R. H. Howe. Air Content of Plastic and Hardened Concrete. Harrisburg, Pennsylvania, Bureau of Materials, Testing, and Research, Pennsylvania Department of Transportation, 1975.

42. Rolfe, S. T. and J. M. Barsom, Fracture and Fatigue Control in Structures. Englewood Cliffs, N. J., Prentice-Hall, Inc., 1977.

43. Shah, S. P. and S. Chandra. "Fracture of Concrete Subjected to Cyclic and Sustained Loading." American Concrete Institute Journal, Proceedings, Vol. 67, No. 10, October 1970, pp. 816-825.

44. Standard Specification for Construction on Primary, Farm to Market, Secondary, State Park, and Institutional Roads and Maintenance Work on the Primary Road System. Iowa State Highway Commission (Iowa Department of Transportation), 1972.

45. Thickness Design for Concrete Pavements. Portland Cement Association, 1966.

46. Troxell, G. E., H. F. Davis and J. W. Kelly. Composition and Properties of Concrete. New York, McGraw Hill Book Co., 1968.

47. Verbeck, G. "Significance of Tests and Properties of Concrete and Concrete Making Materials." American Society for Testing and Materials Special Technical Publication No. 169A., 1966, p. 219.

48. Vesic, A. S. and S. K. Saxena. Analysis of Structural Behavior of AASHO Road Test Rigid Pavements. National Cooperative Highway Research Progress Report No. 97, 1970.

49. Washburn, E. W. "Note on a Method of Determining the Distribution of Pore Size in a Porous Material." Proceedings of the National Academy of Sciences of the United States of America, Vol. 7, 1921, pp. 115-116.

50. Winslow, D. N. and S. Diamond. "A Mercury Porosimetry Study of the Evolution of Porosity in Portland Cement." Journal of Materials, Vol. 5, No. 3, 1970, pp. 564-585.

51. Wuerpel, C. E. Purposeful Entrainment of Air in Concrete. Wilmington, Delaware, Hercules Powder Company, 1970.

52. Yoder, E. J. and M. W. Witczak. Principals of Pavement Design. New York, John Wiley and Sons, Inc., 1975.

53. Yoshimoto, A., S. Ogino and M. Kawakami. "Microcracking Effect on Flexural Strength of Concrete after Repeated Loading." American Concrete Institute Journal, Proceedings, April 1972, pp. 233-240.

8. ACKNOWLEDGMENTS

The study presented in this report was sponsored by the Highway Division of the Iowa Department of Transportation under Research Project HR-183. This study, under the same title, was also supported by and designated as Project 1259 of the Engineering Research Institute, Iowa State University.

The authors wish to extend sincere appreciation to the engineers of Iowa D.O.T. for their support, cooperation, and counseling. A special thanks is extended to Messrs. Bernard Brown and LaVern Huckstadt for their assistance in running the linear transverse and high pressure air tests.

Appreciation is also extended to Dr. Herb T. David, Statistics, for advice on testing sequence for fatigue beams; Dr. Tom McGee, Material Science and Engineering, for use of the concrete specimen polisher and light microscope; Drs. Donald Biggs and Robert Cody, Earth Science, for use of the diamond saw and core drill; and Mr. Jerry Amenson for assistance in the SEM work.

The following individuals contributed, in various capacities, to this investigation: Gary Krupicka, Cheryl Heyveld, Bob Sykes, and S. T. Tong.

9. APPENDIXES

9.1. Appendix A. Material Details

Table A.1 Gradation of fine aggregate.

Sieve Size	% Passing	Iowa D.O.T. Specifications
3/8 in.	100	100
No. 4	96.5	90 - 100
No. 8	76.6	70 - 100
No. 16	56.0	
No. 30	36.1	
No. 50	11.1	
No. 100	0.9	
No. 200	0.4	0 - 1.5

Table A.2. Gradation of coarse aggregate.

Sieve Size	% Passing	Iowa D.O.T. Specifications
1½ in.	100	100
1 in.	96	95 - 100
½ in.	37	25 - 60
No. 4	2	0 - 10
No. 8	1	0 - 5
No. 200	0.4	0 - 1.5

Table A.3. Cement properties.

Property	Test Value	Specification (ASTM C150 and Fed. SS-C-192)
Chemical Data		
MgO	2.6	5.0 max.
SO_3	2.8	3.5 max.
Loss on Ignition	.9	3.0 max.
Insoluable Residue	.2	.75 max.
Physical Data		
Fineness, Blaine, cm^2/gm	3460	2800 min.
Soundness, Autoclave, %	.1	.80 max.
Time of Set, min.		
Vicat, Initial	80	45 min.
Vicat, Final	155	480 max.
Air Content, %	11.0	12.0 max.
Compressive Strength, psi		
3 Day	2480	1800 min.
7 Day	4070	2800 min.

Table A.4. Laboratory batch quantities[a].

Batch	Cement, lb	Water, lb[b]	Sand, lb	Coarse Aggregate, lb	Ad Aire, ml
A	847	382	1890	2314	107
B	968	435	2000	2272	1935
C	968	435	2000	2272	None
D	968	435	2000	2272	968
E	575	259	1188	1350	293

[a]Water-cement ratio = 0.41.

[b]Includes water required to bring aggregates to saturated surface dry condition.

9.2. Appendix B. Test Data

Table B.1. Test data, Batch C, 2.8% air.

Specimen	Modulus of Rupture, psi	% Modulus of Rupture	Fatigue Life, Number of Load Applications for Failure
3-B-10	850	90	80
3-B-22	855	90	40
3-B-24	820	90	1,150
3-B-20	820	90	3,140
3-B-17	900	90	100
3-B-15	870	90	500
3-B-8	860	80	590
3-B-11	880	80	6,110
3-B-26	780	80	29,200
3-B-19	915	80	400
3-B-6	940	80	1,430
3-B-18	910	81	660
3-B-21	820	70	915,240
3-B-23	780	70	319,700
3-B-27	900	70	82,340
3-B-29	860	70	30,980
3-B-13	820	70	97,230
3-B-14	860	65	2,109,950
3-B-16	830	65	2,566,000[a]
3-B-7	886	65	1,053,500
3-B-9	880	60	2,041,200[a]
3-B-25	850	60	2,000,200[a]
3-B-28	870	60	2,642,000[a]
3-B-12	910	60	3,889,100[a]

[a]Failure did not occur.

Table B.2. Test data, Batch A, 3.5% air.

Specimen	Modulus of Rupture, psi	% Modulus of Rupture	Fatigue Life, Number of Load Applications for Failure
4-B-19	770/790		
4-B-21	820/840		
4-B-13	830	90	290
4-B-14	770	90	310
4-B-15	870	90	530
4-B-1	790	85	830
4-B-2	830	85	850
4-B-3	830	85	1,070
4-B-9	850	85	2,100
4-B-10	790	85	1,420
4-B-11	820	85	1,200
4-B-4	810	75	4,880
4-B-5	840	75	2,410
4-B-6	850	75	5,910
4-B-7	870	75	1,010
4-B-8	830	75	10,850
4-B-16	820	65	74,310
4-B-17	890	65	495,460
4-B-18	840	65	2,074,690[a]
4-B-12	820	55	2,721,640[a]

[a]Failure did not occur.

Table B.3. Test data, Batch E, 6.4% air.

Specimen	Modulus of Rupture, psi	% Modulus of Rupture	Fatigue Life, Number of Load Applications for Failure
6-B-19	585	90	630
6-B-8	548	90	580
6-B-5	590	90	1,110
6-B-22	620	90	330
6-B-0	550	90	460
6-B-18	540	80	1,990
6-B-6	533	80	3,670
6-B-4	600	80	6,310
6-B-3	546	80	9,870
6-B-1	600	80	2,830
6-B-20	638	70	5,940
6-B-11	538	70	39,350
6-B-10	548	70	19,280
6-B-16	590	70	22,940
6-B-17	590	70	26,300
6-B-21	643	60	704,830
6-B-7	603	60	144,500
6-B-2	648	60	52,980
6-B-15	600	60	2,200,000[a]
6-B-9	535	60	2,169,790[a]

[a]Failure did not occur.

Table B.4. Test data, Batch D, 10.2% air.

Specimen	Modulus of Rupture, psi	% Modulus of Rupture	Fatigue Life, Number of Load Applications for Failure
10-B-20	460	90	560
10-B-21	495	90	80
10-B-18	440	90	270
10-B-8	490	90	410
10-B-14	506	90	160
10-B-24	483	90	180
10-B-17	490	80	830
10-B-9	445	80	8,810
10-B-11	445	80	16,120
10-B-12	466	80	17,060
10-B-15	460	80	4,100
10-B-7	477	80	1,390
10-B-4	492	80	690
10-B-5	488	80	2,480
10-B-22	500	70	9,080
10-B-19	425	70	82,840
10-B-27	520	70	10,390
10-B-26	506	70	12,390
10-B-6	500	70	8,010
10-B-3	532	70	7,020
10-B-29	495	60	457,810
10-B-16	494	60	2,548,000[a]
10-B-10	471	60	2,652,910[a]
10-B-13	490	60	1,063,510
10-B-23	440	60	3,147,240[a]
10-B-25	520	60	29,860

[a]Failure did not occur.

Table B.5. Test data, Batch B, 11.3% air.

Specimen	Modulus of Rupture, psi	% Modulus of Rupture	Fatigue Life, Number of Load Applications for Failure
11-B-31	440/450		
11-B-30	470/490		
11-B-30A	450/500		
11-B-22	500/540		
11-B-5	480	90	1,440
11-B-14	520	90	240
11-B-9	510	90	90
11-B-2	560	90	100
11-B-23	470	90	360
11-B-20	540	90	50
11-B-3	550	80	460
11-B-15	490	80	3,000
11-B-11	510	80	580
11-B-1	540	80	1,470
11-B-12	540	80	590
11-B-19	530	80	720
11-B-13	510	70	32,970
11-B-16	510	70	277,050
11-B-6	500	70	2,810
11-B-10	498	70	17,980
11-B-18	560	70	8,700
11-B-24	520	70	14,600
11-B-4	560	60	72,250
11-B-17	510	60	2,110,720[a]
11-B-7	470	60	2,000,000[a]
11-B-8	520	60	42,950
11-B-29	540	60	322,380
11-B-21	500	60	1,529,260

[a]Failure did not occur.

9.3. Appendix C. Pavement Design Calculations

Axles during design life - standard PCA design method (45)

Axle Load Groups, Kips	Axle Loads in Design Life
SINGLE	
28-30	3,700
26-28	3,700
24-26	7,410
22-24	195,000
20-22	764,400
18-20	2,139,150
16-18	2,870,400
TANDEM	
52-54	3,700
50-52	3,700
48-50	36,270
46-48	36,270
44-46	57,530
42-44	179,790
40-42	204,750
38-40	296,400
36-38	319,800
34-36	487,500
32-34	610,350
30-32	1,078,350
Total Trucks	19,500,000

CALCULATION OF CONCRETE PAVEMENT THICKNESS
(Use with Case I Single & Tandem Axle Design Charts)

Project Design Example - Iowa DOT (Current PCA Procedure)

Type _____ No. of Lanes _____

Subgrade k 100 pci., Subbase _____

Combined k 130 pci., Load Safety Factor 1.2 (L.S.F.)

PROCEDURE

1. Fill in Col. 1,2 and 6, listing axle loads in decreasing order.
2. Assume 1st trial depth. Use 1/2-in. increments.
3. Analyze 1st trial depth by completing columns 3,4,5 and 7.
4. Analyze other trial depths, varying M.R.*, slab depth and subbase type.**

1	2	3	4	5	6	7
Axle Loads kips	Axle Loads X L.S.F. kips	Stress psi	Stress Ratios	Allowable Repetitions No.	Expected Repetitions No.	Fatigue Resistance Used*** percent

Trial depth 9.5 in. M.R.* 600 psi k 130 pci

SINGLE AXLES

30	36.0	320	.53	240,000	3,700	1.5
28	33.6	300	.50	Unlimited	3,700	

TANDEM AXLES

54	64.8	350	.58	57,000	3,700	6.5
52	62.4	340	.57	75,000	3,700	4.9
50	60.0	330	.55	130,000	36,270	27.9
48	57.6	320	.53	240,000	36,270	15.1
46	55.2	310	.52	300,000	57,530	19.2
44	52.8	300	.50	Unlimited	179,790	

Total 75.1%

* M.R. Modulus of Rupture for 3rd pt. loading.

** Cement-treated subbases result in greatly increased combined k values.

*** Total fatigue resistance used should not exceed about 125 percent.

CALCULATION OF CONCRETE PAVEMENT THICKNESS
(Use with Case I Single & Tandem Axle Design Charts)

Project Design Example - 1933 PCA

Type _____ No. of Lanes _____

Subgrade k 100 pci., Subbase _____

Combined k 130 pci., Load Safety Factor 1.2 (L.S.F.)

PROCEDURE

1. Fill in Col. 1, 2 and 6, listing axle loads in decreasing order.
2. Assume 1st trial depth. Use 1/2-in. increments.
3. Analyze 1st trial depth by completing columns 3, 4, 5 and 7.
4. Analyze other trial depths, varying M.R.*, slab depth and subbase type.**

1	2	3	4	5	6	7
Axle Loads kips	Axle Loads X L.S.F. kips	Stress psi	Stress Ratios	Allowable Repetitions No.	Expected Repetitions No.	Fatigue Resistance Used*** percent

Trial depth 9.5 in. M.R.* 600 psi k 130 pci

SINGLE AXLES

30	36.0	320	.53	77,000	3,700	4.8
28	33.6	300	.50	Unlimited	3,700	

TANDEM AXLES

54	64.8	350	.58	39,000	3,700	9.5
52	62.4	340	.57	43,000	3,700	8.6
50	60.0	330	.55	59,000	36,270	61.5
48	57.6	320	.53	77,000	36,270	47.1
46	55.2	310	.52	88,000	57,530	65.4
44	52.8	300	.50	Unlimited	179,790	

Total 196.9%

* M.R. Modulus of Rupture for 3rd pt. loading.

** Cement-treated subbases result in greatly increased combined k values.

*** Total fatigue resistance used should not exceed about 125 percent.

CALCULATION OF CONCRETE PAVEMENT THICKNESS
(Use with Case I Single & Tandem Axle Design Charts)

Project Design Example - 2.8% Air

Type _____ No. of Lanes _____

Subgrade k 100 pci., Subbase _____

Combined k 130 pci., Load Safety Factor 1.2 (L.S.F.)

PROCEDURE

1. Fill in Col. 1, 2 and 6, listing axle loads in decreasing order.
2. Assume 1st trial depth. Use 1/2-in. increments.
3. Analyze 1st trial depth by completing columns 3, 4, 5 and 7.
4. Analyze other trial depths, varying M.R*, slab depth and subbase type.**

1	2	3	4	5	6	7
Axle Loads kips	Axle Loads X L.S.F. kips	Stress psi	Stress Ratios	Allowable Repetitions No.	Expected Repetitions No.	Fatigue Resistance Used*** percent

Trial depth 9.5 in. M.R.* 700 psi k 130 pci

SINGLE AXLES

30	36.0	320	<.50	Unlimited		
28	33.6	300				
26	31.2					

TANDEM AXLES

54	64.8	350	<.50	Unlimited		
52	62.4	340				
50	60.0	330				
48	57.6	320				
46	55.2	310				
					Total	None

* M.R. Modulus of Rupture for 3rd pt. loading.

** Cement-treated subbases result in greatly increased combined k values.

*** Total fatigue resistance used should not exceed about 125 percent.

CALCULATION OF CONCRETE PAVEMENT THICKNESS
(Use with Case I Single & Tandem Axle Design Charts)

Project Design Example - 6.4% Air

Type _____ No. of Lanes _____

Subgrade k 100 pci., Subbase _____

Combined k 130 pci., Load Safety Factor 1.2 (L.S.F.)

PROCEDURE

1. Fill in Col. 1,2 and 6, listing axle loads in decreasing order.
2. Assume 1st trial depth. Use 1/2-in. increments.
3. Analyze 1st trial depth by completing columns 3,4,5 and 7.
4. Analyze other trial depths, varying M.R.*, slab depth and subbase type.**

1	2	3	4	5	6	7
Axle Loads kips	Axle Loads X L.S.F. kips	Stress psi	Stress Ratios	Allowable Repetitions No.	Expected Repetitions No.	Fatigue Resistance Used*** percent

Trial depth 9.5 in. M.R.* 600 psi k 130 pci

SINGLE AXLES

30	36.0	320	.53	1,200,000	3,700	0.3
28	33.6	300	.50	Unlimited		
26						
24						

TANDEM AXLES

54	64.8	350	.58	170,000	3,700	2.2
52	62.4	340	.57	240,000	3,700	1.5
50	60.0	330	.55	520,000	36,270	7.0
48	57.6	320	.53	1,200,000	36,270	3.0
46	55.2	310	.52	2,000,000	57,530	2.9
44	52.8	300	.50	Unlimited		
					Total	16.9%

* M.R. Modulus of Rupture for 3rd pt. loading.

** Cement-treated subbases result in greatly increased combined k values.

*** Total fatigue resistance used should not exceed about 125 percent.

CALCULATION OF CONCRETE PAVEMENT THICKNESS
(Use with Case I Single & Tandem Axle Design Charts)

Project Design Example - 11.3% Air

Type _____ No. of Lanes _____

Subgrade k 100 pci., Subbase _____

Combined k 130 pci., Load Safety Factor 1.2 (L.S.F.)

PROCEDURE

1. Fill in Col. 1, 2 and 6, listing axle loads in decreasing order.
2. Assume 1st trial depth. Use 1/2-in. increments.
3. Analyze 1st trial depth by completing columns 3, 4, 5 and 7.
4. Analyze other trial depths, varying M.R.*, slab depth and subbase type.**

1	2	3	4	5	6	7
Axle Loads kips	Axle Loads X L.S.F. kips	Stress psi	Stress Ratios	Allowable Repetitions No.	Expected Repetitions No.	Fatigue Resistance Used*** percent

Trial depth 9.5 in. M.R.* 500 psi k 130 pci

SINGLE AXLES

30	36.0	320	.64	8,000	3,700	46.3
28	33.6	300	.60	39,000	3,700	9.5
26	31.2	285	.57	140,000	7,410	5.3
24	28.8	270	.54	850,000	195,000	22.9
22	26.4	250	.50	Unlimited		

TANDEM AXLES

54	64.8	350	.70	800	3,700	462.5
52	62.4	340	.68	1,800	3,700	205.6
50	60.0	330	.66	3,600	36,270	1007.5
48	57.6	320	.64	8,000	36,270	453.4
46	55.2	310	.62	17,000	57,530	338.4
44	52.8	300	.60	39,000	179,790	461.0
42	50.4	287	.57	140,000	204,750	146.3
40	48.0	280	.56	210,000	296,400	141.1
38	45.6	267	.53	1,400,000	319,800	22.8
36	43.2	<250	<.50	Unlimited		
34						

Total 3322.6%

* M.R. Modulus of Rupture for 3rd pt. loading.

** Cement-treated subbases result in greatly increased combined k values.

*** Total fatigue resistance used should not exceed about 125 percent.

CALCULATION OF CONCRETE PAVEMENT THICKNESS
(Use with Case I Single & Tandem Axle Design Charts)

Project Design Example - 1933 PCA

Type _____ No. of Lanes _____

Subgrade k 100 pci., Subbase _____

Combined k 130 pci., Load Safety Factor 1.2 (L.S.F.)

PROCEDURE

1. Fill in Col. 1, 2 and 6, listing axle loads in decreasing order.
2. Assume 1st trial depth. Use 1/2-in. increments.
3. Analyze 1st trial depth by completing columns 3, 4, 5 and 7.
4. Analyze other trial depths, varying M.R.*, slab depth and subbase type.**

1	2	3	4	5	6	7
Axle Loads kips	Axle Loads X L.S.F. kips	Stress psi	Stress Ratios	Allowable Repetitions No.	Expected Repetitions No.	Fatigue Resistance Used*** percent

Trial depth 10.0 in. M.R.* 600 psi k 130 pci

SINGLE AXLES

30	36.0	<300	<.50	Unlimited		
28	33.6					
26	31.2					
24	28.8					
22	26.4					
20	24.0					

TANDEM AXLES

54	64.8	330	.55	59,000	3,700	6.3
52	62.4	320	.53	77,000	3,700	4.8
50	60.0	310	.52	88,000	36,270	41.2
48	57.6	300	.50	Unlimited		
46	55.2					
44	52.8					
42	50.4					
40	48.0					

Total 52.3%

* M.R. Modulus of Rupture for 3rd pt. loading.

** Cement-treated subbases result in greatly increased combined k values.

*** Total fatigue resistance used should not exceed about 125 percent.

CALCULATION OF CONCRETE PAVEMENT THICKNESS
(Use with Case I Single & Tandem Axle Design Charts)

Project Design Example - 2.8% Air

Type _____ No. of Lanes _____

Subgrade k 100 pci., Subbase _____

Combined k 130 pci., Load Safety Factor 1.2 (L.S.F.)

PROCEDURE

1. Fill in Col. 1,2 and 6, listing axle loads in decreasing order.
2. Assume 1st trial depth. Use 1/2-in. increments.
3. Analyze 1st trial depth by completing columns 3,4,5 and 7.
4. Analyze other trial depths, varying M.R.*, slab depth and subbase type.**

1	2	3	4	5	6	7
Axle Loads kips	Axle Loads X L.S.F. kips	Stress psi	Stress Ratios	Allowable Repetitions No.	Expected Repetitions No.	Fatigue Resistance Used*** percent

Trial depth 7.5 in. M.R.* 700 psi k 130 pci

SINGLE AXLES

30	36.0	438	.63	170,000	3,700	2.2
28	33.6	420	.60	740,000	3,700	0.5
26	31.2	396	.57	4,700,000	7,410	0.2
24	28.8	373	.53	710,000,000		
22	26.4	348	< .50	Unlimited		

TANDEM AXLES

54	64.8	480	.69	11,000	3,700	33.6
52	62.4	466	.67	27,000	3,700	13.7
50	60.0	450	.64	100,000	36,270	36.3
48	57.6	440	.63	170,000	36,270	21.3
46	55.2	420	.60	740,000	57,530	7.8
44	52.8	405	.58	2,200,000	179,790	8.2
42	50.4	390	.56	10,000,000	204,750	2.0
40	48.0	375	.54	>10,000,000		
38	45.6	358	.51			
36	43.2	340	<.50	Unlimited		
					Total	124.8%

* M.R. Modulus of Rupture for 3rd pt. loading.

** Cement-treated subbases result in greatly increased combined k values.

*** Total fatigue resistance used should not exceed about 125 percent.

CALCULATION OF CONCRETE PAVEMENT THICKNESS
(Use with Case I Single & Tandem Axle Design Charts)

Project Design Example 6.4% Air

Type _____ No. of Lanes _____

Subgrade k 100 pci., Subbase _____

Combined k 130 pci., Load Safety Factor 1.2 (L.S.F.)

PROCEDURE

1. Fill in Col. 1, 2 and 6, listing axle loads in decreasing order.
2. Assume 1st trial depth. Use 1/2-in. increments.
3. Analyze 1st trial depth by completing columns 3, 4, 5 and 7.
4. Analyze other trial depths, varying M.R.*, slab depth and subbase type.**

1	2	3	4	5	6	7
Axle Loads kips	Axle Loads X L.S.F. kips	Stress psi	Stress Ratios	Allowable Repetitions No.	Expected Repetitions No.	Fatigue Resistance Used*** percent

Trial depth 9.0 in. M.R.* 600 psi k 130 pci

SINGLE AXLES

30	36.0	340	.57	250,000	3,700	1.5
28	33.6	324	.54	850,000	3,700	0.4
26	31.2	305	.51	2,600,000	7,410	0.3
24	28.8	300	<.50	Unlimited		
22	26.4					
20						

TANDEM AXLES

54	64.8	380	.63	30,000	3,700	12.3
52	62.4	365	.61	62,000	3,700	6.0
50	60.0	355	.59	120,000	36,270	30.2
48	57.6	346	.58	180,000	36,270	20.2
46	55.2	330	.55	530,000	57,530	10.9
44	52.8	318	.53	1,300,000	179,790	13.8
42	50.4	308	.51	2,600,000	204,750	7.9
40	48.0	295	<.50	Unlimited		

Total 103.5%

* M.R. Modulus of Rupture for 3rd pt. loading.

** Cement-treated subbases result in greatly increased combined k values.

*** Total fatigue resistance used should not exceed about 125 percent.

17

CALCULATION OF CONCRETE PAVEMENT THICKNESS
(Use with Case I Single & Tandem Axle Design Charts)

Project Design Example 11.3% Air

Type _____ No. of Lanes _____

Subgrade k 100 pci., Subbase _____

Combined k 130 pci., Load Safety Factor 1.2 (L.S.F.)

PROCEDURE

1. Fill in Col. 1, 2 and 6, listing axle loads in decreasing order.
2. Assume 1st trial depth. Use 1/2-in. increments.
3. Analyze 1st trial depth by completing columns 3, 4, 5 and 7.
4. Analyze other trial depths, varying M.R.*, slab depth and subbase type.**

1	2	3	4	5	6	7
Axle Loads kips	Axle Loads X L.S.F. kips	Stress psi	Stress Ratios	Allowable Repetitions No.	Expected Repetitions No.	Fatigue Resistance Used*** percent

Trial depth 10.5 in. M.R.* 500 psi k 130 pci

SINGLE AXLES

30	36.0	276	.55	330,000	3,700	1.1
28	33.6	262	.52	1,100,000	3,700	.3
26	31.2		<.50			

TANDEM AXLES

54	64.8	309	.62	17,000	3,700	21.8
52	62.4	298	.60	40,000	3,700	9.3
50	60.0	290	.58	100,000	36,270	36.3
48	57.6	280	.56	200,000	36,270	18.1
46	55.2	269	.54	500,000	57,530	11.5
44	52.8	261	.52	1,100,000	179,790	16.3
42	50.4	250	<.50			

Total 114.7%

* M.R. Modulus of Rupture for 3rd pt. loading.

** Cement-treated subbases result in greatly increased combined k values.

*** Total fatigue resistance used should not exceed about 125 percent.